行政院國家科學委員會專題研究計畫 成果報告

介觀尺度下氮化鎵量子侷限結構在高 Q 值微共振腔之光子
輻射可控性研究(3/3)
研究成果報告(完整版)

計 畫 主 持 人 ： 王興宗
共 同 主 持 人 ： 孟心飛、彭隆瀚、郭浩中、盧廷昌、林佳鋒
計 畫 參 與 人 員 ： 碩士級-專任助理人員：陳奎廷
　　　　　　　　　 學士級-專任助理人員：邱麗君
　　　　　　　　　 博士班研究生-兼任助理人員：邱清華
　　　　　　　　　 博士班研究生-兼任助理人員：蔡敏安
　　　　　　　　　 博士班研究生-兼任助理人員：邱鏡學
　　　　　　　　　 博士班研究生-兼任助理人員：巫漢敏
　　　　　　　　　 博士班研究生-兼任助理人員：鄭柏孝
　　　　　　　　　 博士班研究生-兼任助理人員：楊仲傑
　　　　　　　　　 博士後研究：李亞儒

報 告 附 件 ： 出席國際會議研究心得報告及發表論文

處 理 方 式 ： 本計畫可公開查詢

中 華 民 國 98 年 11 月 13 日

行政院國家科學委員會補助專題研究計畫 ■ 成 果 報 告
□期中進度報告

Research on Mesoscopic GaN-based Quantum Confined Structures with High-Q Microcavity for Control of Photon Emission

介觀尺度下氮化鎵量子侷限結構在高 Q 值微共振腔之光子輻射可控性研究

計畫類別：■ 個別型計畫　　□ 整合型計畫
計畫編號：NSC97－2120－M－009－001－
執行期間：95 年 08 月 01 日至 98 年 07 月 31 日

計畫主持人：**S.C. Wang** (王興宗)
共同主持人：H.C. Kuo(郭浩中)、L.H. Peng(彭隆瀚)、H.F. Meng(孟心飛)、
　　　　　　T.C. Lu(盧廷昌)、C.F. Lin(林佳鋒)
計畫參與人員：李鎮宇(博士後)、邱麗君(行政助理)，博士生：朱榮堂、
高志強、柯宗憲、邱清華、陳俊榮、陳士偉、羅明華、凌碩均、鄭柏孝、
黃輝閔、蔡閔安、邱鏡學、王朝勳；碩士生：劉亭均、張家銘、卓立夫、
林伯駿、柯智淳、何依嚀、劉玫君、侯延儒、林大為、林詳淇、盧昱昕、
黃重卿、吳永吉、黃柏凱

成果報告類型(依經費核定清單規定繳交)：□精簡報告　■完整報告

本成果報告包括以下應繳交之附件：
□赴國外出差或研習心得報告一份
□赴大陸地區出差或研習心得報告一份
■出席國際學術會議心得報告及發表之論文各一份
□國際合作研究計畫國外研究報告書一份
處理方式：除產學合作研究計畫、提升產業技術及人才培育研究計畫、
　　　　　列管計畫及下列情形者外，得立即公開查詢
　　　　　　　□涉及專利或其他智慧財產權，□一年□二年後可公開查詢

執行單位：國立交通大學
中　華　民　國　　98 年　　10 月　　31 日

Research on Mesoscopic GaN-based Quantum Confined Structures with High-Q Microcavity for Control of Photon Emission

介觀尺度下氮化鎵量子侷限結構在高 Q 值微共振腔之光子輻射可控性研究

PI: S. C. Wang (王興宗), National Chiao Tung University, E-mail:

scwang@mail.nctu.edu.tw

Co-PI: H. C. Kuo (郭浩中), L. H. Peng (彭隆瀚), H. F. Meng (孟心飛), T. C. Lu

(盧廷昌), C. F. Lin (林佳鋒)

中文摘要

　　本研究團隊已完成本三年期研究計畫所規劃之研究目標。包含建立氮化鎵量子局限結構之製程技術、建立理論模型與設計高 Q 值之微共振腔結構與共振腔量子效應、製作含有微共振腔與量子侷限結構之氮化鎵垂直共振腔面射型雷射、研究氮化鎵垂直共振腔面射型雷射元件之特性與製作可控制光子輻射與雷射的氮化鎵垂直共振腔面射型雷射元件。我們發表數種新穎的技術並成功製作世界第一個電激發操作之氮化鎵垂直共振腔面射型雷射。除此之外，我們也成功發表了第一個室溫下光激發之氮化鎵光子晶體面射型雷射，並探討其相關的物理機制與極化特性。另外，利用本研究團隊居於領先地位的高反射率氮化鎵與氮化鋁所組成的佈拉格反射鏡，配合具有高激子束縛能之氧化鋅材料成功製作高 Q 值微共振腔結構，我們研究其光子與激子在量子侷限結構中的交互作用，成功在室溫下觀察到極化子於微共振腔中的存在。因此，本計畫利用不同的奈米製作技術，已成功的使用氮化鎵材料製作出不同型式的微共振腔結構，進而探討不同面向的光子輻射控製機制的可能性。

關鍵詞：氮化鎵、面射型雷射、光子晶體, 微共振腔

英文摘要

We have accomplished the research objectives of this three year project. It includes the establishment of GaN-based quantum confined structures fabrication technology, modeling and design of high Q microcavity and cavity quantum effect, fabrication of GaN vertical cavity surface emitting lasers (VCSELs) with micricavity and quantum confined structures, investigation of performance of the fabricated GaN VCSEL devices, and Demonstration of controlled photon emission and lasing of the GaN VCSEL devices. We have demonstrated several kinds of new technologies and successfully fabricated the first electrically pumped GaN VCSEL. In addition, we have also reported the first room-temperature (RT) optically pumped GaN photonic crystal surface emitting lasers (PCSELs) and discussed the corresponding physical mechanisms and polarization. Moreover, by employing the high-reflectivity GaN/AlN distributed Bragg reflectors (DBRs) developed in our research group, we have fabricated ZnO-based high quality factor (Q) microcavity structures. Because of the strong interaction between photon and exciton in the microcavity, we have observed the microcavity polariton at RT. Therefore, we used different nano-technologies to fabricate many types of microcavity structures and investigated various possibilities about control of photon emission.

Keywords: GaN, VCSEL, Photonic crystal, Microcavity

目錄

報告內容

(一) 前言

An Optical microcavity consists of two high-reflectivity mirrors and a thin active layer in which photons are confined in small volumes by resonant recirculation. Microscale cavity ensures that the resonant frequencies are sparsely distributed throughout the spectrum and can be controlled by changing the cavity volume. Microcavities made of active III-V semiconductor materials can control emission spectra, which has been widely used in the fabrication of vertical cavity surface emitting lasers (VCSELs) and resonant cavity light emitting diodes (RCLEDs). In addition to the planar-type microcavities, microcavities based on photonic crystals can provide extremely small mode volumes. A photonic crystal (PC) is a bulk spatially periodic structure whose dielectric constant is modulated with a period comparable to the light wavelength. The interaction between such a crystal and photons essentially modifies the spatial distribution and the energy spectrum of the electromagnetic field; it means that the photonic crystal can be engineered to possess a photonic band gap (PBG) for a specific range of frequencies for which electromagnetic waves are forbidden to exist within the crystal. Based on a appropriate design of photonic crystal lattices and the use of active layer, photonic crystal surface emitting lasers (PCSELs) can be achieved and provide a large area single mode laser. Beyond the standard applications of the surface emitting lasers, microcavity polariton is another hot topic in recent year. Photons and excitons can be confined in a semiconductor microcavity simultaneously. Under this condition, when the cavity photon mode is resonant with an exciton mode, the strong coupling regime is achieved and the new coupled modes, named cavity polaritons are created. microcavity polaritons are admixed quasiparticles originated from the strong interaction between cavity photons and excitons. The half matter-half light nature of the Bose particles provides the extremely light effective mass and the controllable exciton-polariton dispersion curves by designing different cavity-exciton detuning values. These unique MC polariton properties are very important for the study of the fundamental physical phenomena including strong light-matter interaction, solid-state cavity quantum electrodynamics, and dynamical Bose-Einstein condensates (BEC). In this research report, we will focus on the investigation and development of above applications from semiconductor microcavities. Our research results in three years about VCSELs, PCSELs, microcavities, and nanotechnology on LEDs will be reviewed in detail. The related publications about the research results of GaN-based VCSELs, PCSELs, microcavities, and nanostructure GaN LEDs are also listed in this report for the readers to obtain the detailed information.

(二) 研究目的

1. GaN-based vertical-cavity surface-emitting lasers (VCSELs)

VCSELs have many inherent advantages, such as circular output beam, low beam divergence, high modulation bandwidth, single longitudinal mode, and convenient wafer-level testing [1]–[3]. These advantages make VCSELs promising optoelectronic devices for many practical applications, such as high density optical storage system, laser printing, free space optical interconnects, fiber-optic communications, etc. Conventional GaAs- and InP-based red and infrared VCSELs have been commercialized for a long time due to its lattice-matched DBRs and suitable GaAs and InP substrates. However, the development of GaN-based VCSELs is relatively slow even though the idea of such a VCSEL has been proposed by Iga et al. since 1979 [4]. GaN and its most relevant alloys such as InGaN and AlGaN have many unique properties suitable for fabrications of various photon emission devices including LEDs and edge-emitting laser diodes (LDs). By varying the alloy composition, different photon emission can be obtained over a wide range of energy from 0.7 to 6.2 eV, covering the wavelength range from infrared to ultraviolet. However, there are several key technical issues in realization of nitride-based laser devices. These include no suitable GaN substrate material, difficulty in p-doping, and relatively high defect densities of epitaxially grown films, limiting the development of GaN-based optoelectronic devices. As for GaN-based VCSELs, the lasing action of GaN-based VCSELs is mostly reported under optical pumping conditions. There are three critical difficulties in fabricating electrically pumped GaN VCSELs. One is the lack of suitable substrates, leading to much higher defect densities in GaN films. Another is the difficulty in growing high-quality and high-reflectivity GaN-based DBRs due to the large lattice mismatch between GaN and AlN layers. The other is to obtain low-resistive p-type GaN layers, originated from the high activation energy of Mg dopants. Despite the material quality or fabrication problems, our research group was still devoted to the study of GaN-based VCSELs. Based on our previous research results about the improvement of high-reflectivity GaN/AlN DBRs [5], we have successfully demonstrated optically pumped GaN VCSELs at RT and electrically pumped GaN VCSELs at 77 K.

2. GaN-based photonic crystal surface-emitting lasers (PCSELs)

During the past decade, photonic crystals (PCs) have drawn much attention, and have many advantages to control the light propagation and photonic bandgap. The applications of PCs nanostructure can function as good photonic devices [6]–[8]. In general, there are two types of PC lasers, which have been developed and investigated. The first one fabricates a PC defect with an optical gain surrounded by 2-D or 3-D PC mirrors to form a resonant cavity, and lasing actions arise from the resonant cavity modes with high Q-values and a small modal volume. This kind of microcavity laser can achieve strong Purcell effect and the low-threshold lasing [9], [10]. Another type of PC lasers can operate without any defined cavity and extrinsic mirror because Bloch waves have an intrinsic feedback mechanism near the bandgap edge. Thus, this kind of PC laser is called as the band edge laser. The multidirectional distributed feedback effect near the band edges in two-dimensional (2D) PC structures can create a surface emitting laser [11], [12]. This kind of PC surface emitting lasers (PCSELs) could be considered as a candidate for perfect single

mode emission over a large area, high output power, and surface emission with narrow divergence angle [13], [14]. These PCSEL structures are usually composed of a perfect PC lattice and the laser action would happen in those band edge points in the photonic band diagram by satisfying the Bragg condition. The surface emission would occur when the vertical diffraction conditions are satisfied. Due to the advantages of the nitride-based materials, we focused our attention on the research topic of GaN-based PCSELs. The lasing action of GaN PCSELs was observed at RT by optical pumping technique. The corresponding laser performance and characteristics are also discussed in this report.

3. Semiconductor microcavity polaritons

Semiconductor microcavities have recently gained intense interest in the research of strong light-matter interaction since the pioneering work of Weisbuch *et al.* in 1992. [15]. In microcavity structure with strong interaction of excitons and photons, the new quasiparticles termed cavity polaritons are created and characterized by bosonic properties including very light mass and controllable dispersions. These unique MC polariton properties provide the possibility to investigate the fundamental physical phenomena including strong light-matter interaction, solid-state cavity quantum electrodynamics (CQED), and dynamical BEC. Besides, further applications of microcavity polaritons include polariton lasers [16], polariton light-emitting diodes [17], and polariton parametric amplifiers [18]. The first experimental observation of strong coupling regime confirmed by an anticrossing of the exciton and photon modes was reported in a GaAs-based microcavities [15]. Because of the nearly lattice-matched AlGaAs/AlGaAs DBRs and the high-quality GaAs/AlGaAs quantum wells (QWs), the growth and fabrication of GaAs-based semiconductor microcavities with high-quality factor (Q) are relatively easy. Consequently, the investigation of GaAs-based microcavity polariton has been widely reported and the electrically driven polariton LEDs are also demonstrated [17], [19]. Nevertheless, polariton optoelectronic devices operating at high temperatures require wide-bandgap material systems which can provide larger exciton binding energy than GaAs and can assure the existence of excitons at that temperature. In this sense, nitride-based material systems have attracted much attention in this research field due to their large exciton binding energy of about 26 meV for GaN bulk layers [20] and about 40–50 meV for GaN-based QW structures due to the quantum confinement effect [21]. Furthermore, ZnO-based microcavity is an attractive alternative for the study of polariton-related properties at RT since the exciton binding energy is as even larger about 60 meV for bulk ZnO layers. Therefore, based on our previous research results about the high-reflectivity AlN/GaN DBRs [5], we have fabricated ZnO-based microcavity structure and successfully observed the strong light-matter interaction. The cavity Q value is about 250, which is the state of the art for a ZnO-based microcavities and has a large vacuum Rabi splitting of about 72 meV. The detail research results will be shown in this report.

(三) 文獻探討

1. Recent development of GaN-based VCSELs

The fabrication of GaN-based VCSEL is a significant challenge due to the difficulty of growing high-reflectivity nitride-based DBRs. Despite the material quality and fabrication problems, realizations of the GaN-based VCSELs have been reported. The first demonstration of the RT optically pumped GaN-based VCSELs has been reported by Redwing *et al.* in 1996 [22]. The fully epitaxial VCSEL structure consists of a 10 μm GaN active region sandwiched between 30-period $Al_{0.12}Ga_{0.88}N$/ $Al_{0.4}Ga_{0.6}N$ DBRs with the reflectivity values about 84~93% from the theoretical prediction. The relatively low reflectivity results in the high threshold pumping energy ~2.0 MW/cm^2 and the employment of thick GaN gain layer. Furthermore, Arakawa *et al.* fabricated an $In_{0.1}Ga_{0.9}N$ VCSEL and observed the lasing action at 77 K for the first time in 1998 [23]. The 3-λ cavity comprising an $In_{0.1}Ga_{0.9}N$ active layer was grown on 35-pair $Al_{0.34}Ga_{0.66}N$/GaN DBRs with the reflectivity of 97%. The top-DBR consisting of 6-pair TiO_2/SiO_2 multi-layer providing the reflectivity of 98% was evaporated on the top of the active layer to form the hybrid VCSEL structure (i.e., the VCSEL structure consisting of semiconductor grown mirror and dielectric deposited mirror). The emission linewidth significantly decreased from 2.5 nm to 0.1 nm after the threshold condition. Thereafter, Song *et al.* demonstrated a VCSEL structure consisting of InGaN multiple quantum wells (MQWs) and 10-pair SiO_2/HfO_2 top and bottom DBR by using laser left-off technology in 1999 [24]. Since the reflectivity of top and bottom DBRs were 99.5 and 99.9% respectively, the cavity *Q* factor is larger than 600 in their experiments. In the same year, Someya *et al.* reported the RT lasing at blue wavelengths in hybrid GaN-based VCSELs [25]. Lasing action was observed at a wavelength of 399 nm under optical excitation and the emission linewidth decreased from 0.8 nm below threshold to less than 0.1 nm above threshold. In 2005, crack-free fully epitaxial nitride microcavity using lattice-matched AlInN/GaN DBRs has been reported by Carlin *et al.* [26]. The optical cavity was formed by a 3λ/2 GaN cavity surrounded by lattice-matched AlInN/GaN DBRs with reflectivity values close to 99%. The cavity mode was clearly resolved with a linewidth of 2.3 nm. However, the laser behavior has not been reported in this kind of VCSEL structure at that time. Other optically pumped results reported in recent years are aimed at improving the device performance and investigating the physical mechanisms [27–34]. It was not until 2008 that the first electrically pumped GaN VCSEL was demonstrated at 77 K under CW operation by our group [35] and recently the RT CW GaN VCSEL was also reported by Nichia Corporation [36].

2. Recent development of GaN-based PCSELs

The PCSELs have been demonstrated by many research groups in recent years. Kwon *et al.* reported RT optical pumping of photonic crystal air-bridge slabs lasers by using InGaAsP QWs emitting at 1.5 μm in 2003 [37]. A low threshold incident pump power of less than 1 mW is achieved for the laser operating at the second bandedge near the X and M points, with only 15×15 lattice points. The measured characteristics of the bandedge lasers closely agree with the result of calculations based on the plane-wave-expansion method and the finite-difference time-domain method. In addition to the InP-based materials, Notomi *et al.* demonstrated a series of

two-dimensional (2D) hexagonal organic photonic-crystal lasers whose lattice constant varies from 0.18 to 0.44 μm, and observed clear lasing oscillation at the four lowest band gap frequencies [38]. They used in-plane beam propagation analysis to clarify the 2D feedback mechanism at each gap frequency, which differs for different gaps. Theobserved K_1 lasing oscillation is due to coupling of three nonparallel diffracted waves, which has a purely 2D character. Furthermore, Noda's group published electrically pumped GaN-based PCSELs at blue-violet wavelength at RT in 2008 [39]. They have developed a fabrication method, named "air holes retained over growth," in order to construct a two-dimensional GaN/air PC structure. The resulting periodic structure has a PC band-edge effect sufficient for the successful operation of a current-injection surface-emitting laser. Our research approaches to the fabrication of GaN PCSELs are based on the combination of AlN/GaN DBRs and PC bandedge effects. RT optically pumped GaN PCSELs have been demonstrated in our research results and will be presented in the following sections.

3. Recent development of semiconductor microcavity polaritons

The first experimental observation of strong coupling regime confirmed by an anticrossing of the exciton and photon modes was reported in a GaAs-based MC [15]. Thereafter, many research groups are devoted to this research field and the related literatures have been reported in recent years. Tsintzos et al. demonstrated a electrically pumped GaAs-based polariton LEDs, which emits directly from polariton states at a temperature of 235 K. Polariton electroluminescence data reveal characteristic anticrossing between exciton and cavity modes, a clear signature of the strong coupling regime. The first experimental results of the strong coupling regime in GaN-based MCs were reported by Antoine-Vincent et al. in 2003 [40]. RT polariton lasing in a bulk GaN MC under nonresonant pulsed optical pumping has been demonstrated by Christopoulos et al. [41]. The $3\lambda/2$ bulk GaN cavity was sandwiched between a bottom 34 pair $Al_{0.85}In_{0.15}N/Al_{0.2}Ga_{0.8}N$ DBR and a top 10 pair SiO_2/Si_3N_4 DBR. The Q factor obtained was ~ 2800. Further challenging RT strong coupling regime and nonlinear effects in GaN-based QWs microcavities were studied. Christmann et al. employed GaN-based hybrid microcavities which consist of a 3λ cavity layer with 67 period of $GaN/Al_{0.2}Ga_{0.8}N$ MQWs sandwiched between a 35 pair of lattice-matched $Al_{0.85}In_{0.15}N/Al_{0.2}Ga_{0.8}N$ DBR and a 10 pair SiO_2/Si_3N_4 DBR. The vacuum Rabi splitting of 56 meV is observed at RT. Furthermore, ZnO-based MC is an attractive alternative for the study of polariton-related properties at RT since the exciton binding energy is as even larger about 60 meV for bulk ZnO layers. Theoretical analysis has expected that a bulk ZnO MC is a potentially excellent candidate for the realization of room-temperature (RT) polariton lasers [42], [43]. Consequently, several experimental results about ZnO MCs have been reported in recent years [44]-[47]. Schmidt-Grund et al. demonstrated MC structures with ZnO as the cavity surrounded with ZrO_2/MgO DBRs. The maximum Rabi splitting value about 78 meV was estimated from the coupling of the excitons and the Bragg band-edge modes. Besides, Nakayama et al. reported a MC consisting of a ZnO active layer and HfO_2/SiO_2 DBRs at the bottom and top. The Rabi splitting energy was estimated to be ~80 meV at 10 K. Nevertheless, this kind of double dielectric DBR MCs may easily suffer the degradation

of ZnO crystal quality and be found to be polycrystalline. Furthermore, Médard *et al.* reported hybrid ZnO MCs with bottom 7.5-pair $Al_{0.2}Ga_{0.8}N/AlN$ DBR grown on Si(111) substrates and 10 nm aluminum top mirrors [44]. The maximum Rabi splitting of about 70 meV was obtained at 5 K. Shimada *et al.* demonstrated another kind of hybrid MCs composed of 29-pair $Al_{0.5}Ga_{0.5}N/GaN$ DBR at the bottom of the ZnO cavity layer and 8-pair SiO_2/Si_3N_4 DBR as the top mirror [45]. The Rabi splitting was estimated to be ~50 meV at RT. In our research results, we have fabricated a high Q ZnO-based microcavity and the vacuum Rabi splitting is of about 72 meV.

(四) 研究方法、結果與討論

1. Research results of GaN-based VCSELs

The evolution of nitride-based light-emitting devices suffered many obstacles, such as the absence of lattice-matched substrates [48], low activation ratio of p-type (Al)GaN , large mobility difference between electrons and holes, crystal-structure- and strain-induced quantum-confined-Stark effect (QCSE), etc. These problems have been widely investigated in nitride-based LEDs and LDs. Nevertheless, the most difficult challenge for nitride-based VCSELs is the lattice-mismatched nitride-based DBRs. High-quality and high-reflectivity DBRs are necessary to achieve threshold condition due to the relatively short gain region of a VCSEL. In general, there are three kinds of material systems used in nitride-based DBRs, including AlN/GaN, Al(Ga)N/(Al)GaN, and AlInN/GaN. The AlN/GaN DBRs offer the highest refractive index contrast among the III-nitride compounds and provide highly reflective structures together with a large stopband width. However, the large lattice mismatch between AlN and GaN is up to 2.4%, which generally results in a tensile strain and the formation of cracks. These cracks tend to grow into V-shaped grooves and seriously affect the reflectivity of the DBR due to scattering, diffraction, and absorption. To prevent the formation of cracks, the $Al_xGa_{1-x}N/Al_yGa_{1-y}N$ system is usually used to reduce the strain in the whole DBR structure. Nevertheless, the refractive index contrast decreases with increasing Al composition in GaN or Ga composition in AlN, which leads to a reduced stopband width and the requirement of increased number of pairs to achieve high reflectivity. An alternative approach was proposed by Carlin and Ilegems [49]. They demonstrated high-reflectivity AlInN/GaN DBRs near lattice matched to GaN. The 20-pair DBRs exhibited a peak reflectivity over 90 % and a 35 nm stopband width at 515 nm. Although this kind of DBR has been reported, the growth of high-quality AlInN film is difficult due to the composition inhomogeneity and phase separation in AlInN, which results from large mismatch of covalent bond length and growth temperature between InN and AlN.

In order to obtain high-reflectivity and large-stopband DBRs for nitride-based VCSELs, our group is keeping on the study of growing high-quality AlN/GaN DBRs. In our previous study, we reported the growth of crack-free AlN/GaN DBRs with insertion of 5.5 periods of AlN/GaN superlattice (SL) [5]. Fig. 1 shows cross-sectional transmission electronic microscopy (TEM) images of the SL DBR structure. The lighter layers represent AlN layers while the darker layers

represent GaN layers. The interfaces between AlN and GaN layers are sharp and abrupt in low-magnification TEM image, as shown in Fig. 1(a). The arrows indicate the SL insertion positions. Fig. 1(b) shows the cross-sectional TEM image of one set of 5.5-pairs AlN/GaN SL insertion layers under high magnification. Detailed observations by this TEM image reveal that the V-shaped defects in the AlN layers are always observable at the GaN-on-AlN interfaces and filled in with GaN. These V-shaped defects have been reported earlier and could be due to various origins such as stacking mismatch boundaries and surface undulation. The GaN/AlN SL insertion layers were ended by one more AlN layer to identify the changing from the AlN layer to the GaN layer. Here a set of GaN/AlN SL insertion layers can be seen as a quasi alloy of an $Al_xGa_{1-x}N$ layer for a low refractive index quarter-wave layer in the DBR structure. The effect of the SL insertion layers on the structural characteristics of the nitride DBRs is relevant to the mechanism of strain relaxation. The relaxation process of AlN/GaN SL layers keeps relatively better coherency, i.e., GaN and AlN SL layers are fully strained against each other. Therefore, the SLs behave like effective bulk layers which have in-plane lattice constant between bulk GaN and AlN DBR layers. The subsequent growth of five-pair AlN/GaN DBR could follow the AlN/GaN SLs, which will make the DBR layers suffer relatively smaller strain as compared with DBR layers grown on bulk GaN layer. Consequently, the insertion of the SL layers during the growth of the DBR layers could act as strain buffers between DBRs and the underlying GaN bulk layer because the in-plane lattice constants of the SL layers are close to those of the AlN layers in the DBRs.
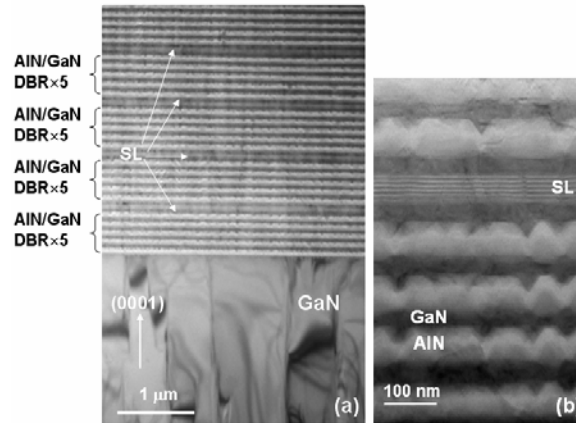
Fig. 1. Low-magnification cross-sectional TEM image of the SL DBR structure. (b) High-magnification cross-sectional TEM image of the SL DBR structure. The 5.5-pair AlN/GaN SL can be observed clearly

Another consideration of the VCSEL design is the thickness and position of the InGaN/GaN MQWs inside the GaN microcavity. Typically, the cavity length of VCSELs is on the order of few half operating wavelengths. In such a short cavity device, the electromagnetic waves would form standing wave patterns with nodes (electromagnetic wave intensity minima) and anti-nodes (electromagnetic wave intensity maxima) within the GaN microcavity. The location of the InGaN/GaN MQWs with respect to the anti-modes can significantly affect the coupling of laser mode with the cavity field. The proper alignment of the MQWs region with the anti-nodes of the cavity standing wave field patterns will enhance the coupling and reduce laser threshold condition. As a result, the precise layer thickness control in the VCSEL fabrication is important.

Wang's group used ten pairs InGaN/GaN MQWs to form a $1/2\lambda$ optical thickness to fully overlap with one standing wave pattern in order to have a more thickness tolerance during the fabrication and to have a higher longitudinal confinement factor with respect to the total cavity length. Fig. 2 shows the refractive index value in each layer and the simulated standing wave patterns inside the hybrid DBR VCSEL structure. Since the bottom AlN/GaN DBR and the GaN cavity are epitaxially grown, the precise layer thickness can be controlled by the *in-situ* monitoring system. By fixing a specific monitor wavelength, the thickness of each quarter-wavelength GaN and AlN, and GaN cavity can be precisely controlled by following the reflectance signals during the metal organic chemical vapor deposition (MOCVD) growth. The total reflectance signal at 460 nm for the half-cavity structure is shown in Fig. 3 The relative reflectivity is gradually saturated with increasing number of DBR pairs, as shown in Fig. 3(a). The AlN/GaN SL layers are inserted in to AlN/GaN DBR at the time indicated as SL. The cavity thickness and positions of MQWs can also be *in-situ* monitored by observing the oscillation periods during the growth, as shown in Fig. 3(b). After the growth of nitride-based half cavity, an eight-pair of Ta_2O_5/SiO_2 dielectric mirror was deposited by electronic beam evaporation as the top DBR reflector to form the hybrid microcavity.
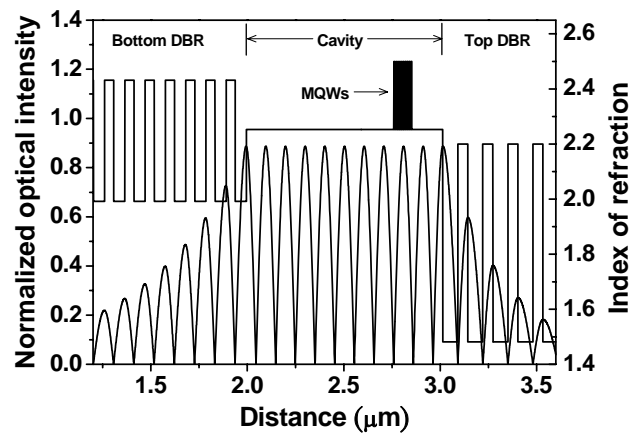
Fig. 2. Schematic representation of the relation between refractive index and longitudinal optical field for a typical hybrid DBR VCSEL.

Because of the difficulty of growing high-quality and high-reflectivity nitride-based DBRs, the possible design of GaN based blue-VCSELs has been proposed by Iga in 1996 [50]. The corresponding structural designs for nitride-based VCSELs can be classified into three major types, as shown in Fig. 4. The first one is monolithic grown vertical resonant cavity consisting of epitaxially grown III-nitride top and bottom DBRs [Fig. 4(a)]. The advantage of the fully epitaxial microcavity is the controllable cavity thickness which is beneficial to fabricate microcavity structure. However, VCSELs require extremely high-reflectivity DBRs (i.e., high cavity Q factor). The fully epitaxial nitride microcavity is very difficult to achieve this requirement. The second one is vertical resonant cavity consisting of dielectric top and bottom DBRs [Fig. 4(b)]. The double dielectric DBR VCSELs can exhibit high cavity Q factors because of the high-reflectivity DBR, which are relatively easy to fabricate. The large refractive index contrast in dielectric materials can make high-reflectivity and large-stopband DBR with less number of pairs. The drawback of the double dielectric DBR VCSEL is the difficulty of

controlling the cavity thickness precisely and the complicated fabrication process due to the employment of laser lift-off technique [51]. In addition, the thickness of the GaN cavity should keep as thick as possible to avoid the damage of the InGaN/GaN MQWs during the laser lift-off process. Such a thick cavity length could increase the threshold condition and reduce the microcavity effect. Although the cavity layer can be polished and thinned using chemical-mechanical polishing (CMP) technique, the smooth surface is another key issue for high-quality GaN cavity. The third one is the VCSEL structure combining an epitaxially grown DBR and a dielectric type DBR which compromises the advantages and disadvantages of the above two VCSEL structures [Fig. 4(c)]. The hybrid DBR VCSEL can eliminate the complex process and keep the feasibility of coplanar contacts with dielectric DBR mesas for the future electrically pumped VCSEL applications. The major requirement for the fabrication of hybrid DBR VCSEL is to grow high-reflectivity and high-quality nitride-based DBRs. Our approaches to the realization of GaN-based VCSELs are mainly based on the double dielectric DBR VCSELs and the hybrid DBR VCSELs. The device performances of these two VCSEL structures will be analyzed and discussed in the following sections.
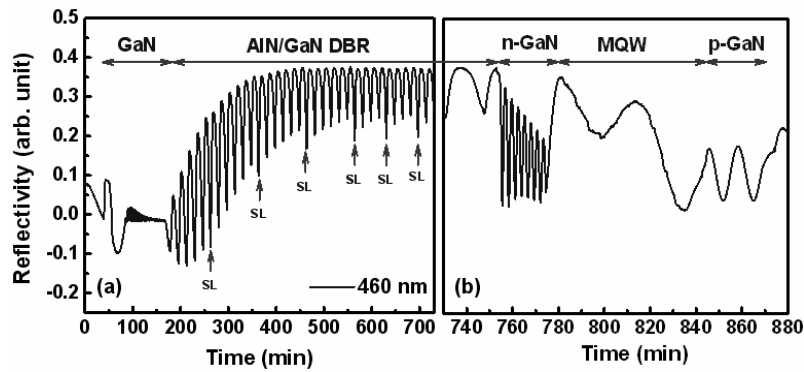

Fig. 3. (a) In-situ normal reflectance measurement during the growth of the AlN/GaN DBR and GaN microcavity with InGaN/GaN MQWs by a fixed measurement wavelength of 460nm. The AlN/GaN superlattices are inserted into AlN/GaN DBR at the time indicated as SL. (b) Enlarged part of reflectance signals during the growth of the GaN microcavity consisted of n-GaN, InGaN/GaN MQWs and p-GaN layers.
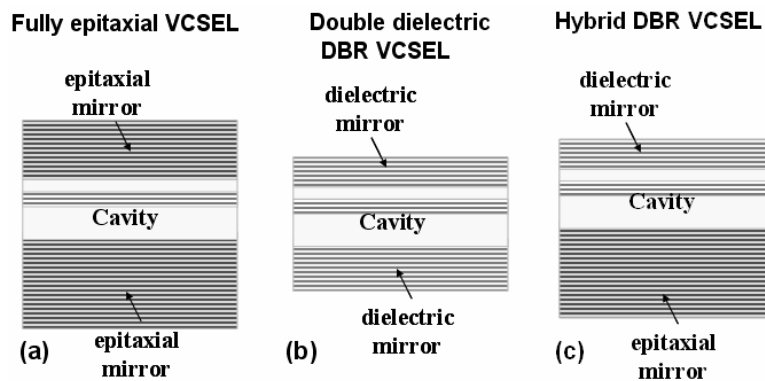

Fig. 4. Three kinds of GaN-based VCSEL structures. (a) Fully epitaxial VCSELs. (b) Double dielectric DBR VCSELs. (c) Hybrid DBR VCSELs

1. (a) Research results about optically pumped GaN-based VCSELs

9

The hybrid DBR GaN-based VCSELs were grown in a low-pressure high-speed rotating-disk MOCVD system. Two-inch diameter (0001)-oriented sapphire substrates were used for the growth of AlN/GaN DBR and cavity. During the growth, trimethylgallium (TMGa), trimethylindium (TMIn), and trimethylaluminum (TMAl) were used as group III source materials and ammonia (NH$_3$) as the group V source material. Then, the growth process was as follows. The substrate was thermally cleaned in hydrogen ambient for 5 min at 1100°C, and then a 30 nm thick GaN nucleation layer was grown at 500°C. The growth temperature was raised up to 1100°C for the growth of a 2-µm GaN buffer layer. Then the 29 pairs of AlN/GaN DBR with six AlN/GaN superlattice insertion layers were grown under the fixed chamber pressure of 100 Torr. In order to reduce the tensile strain between the AlN and GaN, they inserted one superlattice into each five DBR periods at first twenty pairs of DBR. Then the superlattice was inserted into each three DBR periods for the remaining nine pairs of DBR to reduce the tensile strain. The overall AlN/GaN DBRs has 29 pairs with six superlattice insertion layers. On top of this 29-pair AlN/GaN DBR is a 790-nm-thick Si-doped n-type GaN cladding layer. The MQW active region consists of ten 2.5-nm-thick In$_{0.2}$Ga$_{0.8}$N QWs and 7.5-nm-thick GaN barrier layers. A 120-nm-thick Mg-doped p-type GaN cladding layer was grown on top of the MQWs to form a 5λ cavity in optical thickness for center wavelength of 460 nm. Here, they chose 460 nm as the designed lasing wavelength mainly due to the consideration of the higher absorption of the indium tin oxide (ITO) layer at shorter wavelength for the further electrically pumped GaN VCSELs. Besides, the grown epilayer thickness is easier to monitor at this wavelength by the *in-situ* monitor system. After the growth of nitride-based half cavity, an eight pairs of Ta$_2$O$_5$/SiO$_2$ dielectric mirror was deposited by electronic beam evaporation as the top DBR reflector to form the hybrid microcavity.

The experimental results obtained from the performance characteristics of optically pumped VCSELs provide useful information for further development of electrically pumped VCSELs. It allows the estimation of the threshold condition of the designed VCSEL structure and provides better understanding of the material properties. From the reflectivity spectrum of the full VCSEL structure, the accuracy of the cavity thickness can be assured. Fig. 5 shows the RT reflectivity spectrum of whole microcavity under near normal incidence. The peak reflectivity is about 97 % with a large stopband of 70 nm originated from the large refractive index contrast between Ta$_2$O$_5$ and SiO$_2$ layers. The irregular long wavelength oscillations of the reflectivity spectrum arise from the modulation of the respective top and bottom DBR spectra. On the other hand, the short wavelength oscillator is relatively regular, which only results from the top dielectric DBR since the short-wavelength light is absorbed by GaN layer. The photoluminescence (PL) emission spectrum of the full microcavity was measured at room temperature and shown in Fig. 5 as well. The excitation source is a 325-nm He-Cd laser and the cavity resonance mode at 464.2 nm with a full-width at half-maximum (FWHM) value of 0.61 nm is clearly observed. The cavity mode dip is located at reflectivity curve corresponding to the emission peak. This indicates that the InGaN/GaN MQWs emission peak was well aligned with the hybrid microcavity. The cavity Q factor was estimated from the λ/Δλ to be about 760.
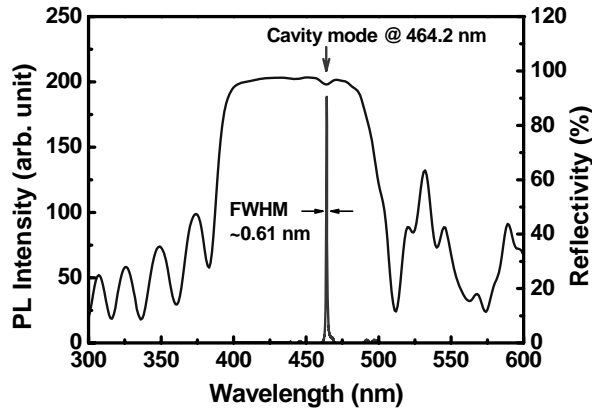
Fig. 5. Room-temperature reflectivity spectrum and PL spectrum of whole GaN-based microcavity

To examine the lasing action, they measured the emission intensity of the hybrid microcavity with increasing pumping power using a microscopic optical pumping system. The optical pumping of the samples was performed using a frequency-tripled Nd:YVO$_4$ 355-nm pulsed laser with a pulse width of ~0.5 nm at a repetition rate of 1 kHz. The pumping laser beam with a spot size ranging from 30 to 60 μm was incident normal to the VCSEL sample surface. The light emission from the VCSEL sample was collected using an imaging optic into a spectrometer/CCD (Jobin-Yvon Triax 320 Spectrometer) with a spectral resolution of ~0.1 nm for spectral output measurement. Fig. 6 shows the emission intensity at RT from the hybrid GaN-based VCSEL as a function of the excitation energy. A distinct threshold characteristic can be found at the threshold excitation energy of ~55 nJ corresponding to an energy density of 7.8 mJ/cm^2. Then the laser output increased linearly with the pumping energy beyond the threshold. A dominant laser emission line at 448.9 nm appears above the threshold pumping energy.
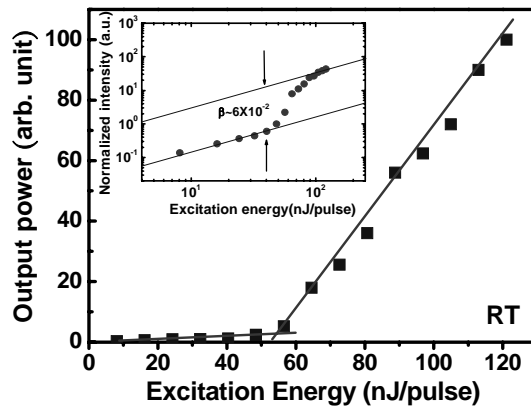

Fig. 6. Laser emission intensity as a function of the exciting energy at room temperature conditions for the hybrid DBR VCSEL. (Inset) Laser emission intensity versus pumping energy in logarithmic scale. The difference between the heights of the emission intensities before and after the threshold corresponds roughly to the value of β. The dash lines are guides for the eye.

The laser emission spectral linewidth reduces as the pumping energy above the threshold energy and approaches 0.17 nm at the pumping energy of 82.5 nJ. In order to extract the spontaneous coupling factor β of this cavity from Fig. 6, they normalized the vertical scale and re-plotted it in a logarithm scale as shown in the inset in Fig. 6. The difference between the

heights of the emission intensities before and after the threshold roughly coincides with the value of β. The β value of this hybrid GaN-based VCSEL estimated from the inset of Fig. 6 is about 6×10^{-2}. The alternative approach to estimating the β value is based on the approximation equation which can be expressed by

$$\beta = \frac{F_p}{1+F_p} \tag{1.1}$$

with

$$F_p = \frac{3}{4\pi^2} \frac{Q}{V_c/(\lambda/n)^3} \tag{1.2}$$

where F_p is the Purcell factor, Q is the cavity quality factor, λ is the laser wavelength, V_c is the optical volume of laser emission, and n is the refractive index. Since the photoluminescence spectrum of the hybrid DBR VCSEL showed a narrow emission peak with FWHM of 0.61 nm, cavity quality factor was estimated to be 760. The refractive index is 2.45 for the GaN cavity. For the estimation of the optical volume, they used the spot size of the laser emission image which was about 3 μm and the cavity length of about 9.5λ with considering the penetration depth of the DBRs. By using these parameters, the Purcell factor of about 2.9×10^{-2} was obtained and they estimated the β value to be about 2.8×10^{-2}, which has the same order of magnitude as the above β value estimated from the inset in Fig. 6. This β value is three order of magnitude higher than that of the typical edge emitting semiconductor lasers (normally about $10^{-4} \sim 10^{-5}$ [52]) indicating the enhancement of the spontaneous emission into a lasing mode by the high quality factor microcavity effect in the VCSEL structure. The variation of the laser emission intensity with the angle of the polarizer was also measured and showed nearly a cosine square variation. The result shows that the laser beam has a degree of polarization of about 89%, suggesting a near linear polarization property of the laser emission.

The schematic fabrication flowchart for dielectric DBR VCSELs is shown in Fig. 7. The layer structure of the GaN-based cavity, grown on a (0001)-oriented sapphire substrate by MOCVD is described as followed: a 30-nm nucleation layer, a 4-μm GaN bulk layer, MQWs consisting of 10 periods of 5-nm GaN barriers and 3-nm $In_{0.1}Ga_{0.9}N$ wells, and a 200-nm GaN cap layer. The peak emission wavelength of the MQWs for the as-grown sample was obtained to be 416 nm. Then, the dielectric DBR consisting of 6-pair SiO_2/TiO_2 was evaporated on the top of GaN-based cavity. The stop band center of the DBR was tuned to 450 nm. The reflectivity of the SiO_2/TiO_2 DBR at 414 nm is obtained to be 99.5%. Next, in order to enhance the adhesion between the epitaxial layers and silica substrate, an array of disk-like patterns with the diameter of 60 μm was formed by standard photolithography process and the SiO_2/TiO_2 DBR mesas were formed by the buffer oxide etcher. The wafer was then mounted onto a silica substrate, which is nearly transparent to the wavelength of the excitation light and the VCSEL. A KrF excimer laser radiation at 248 nm was guided into the sample from back side of the sapphire to separate the sapphire from the epitaxial layers [53]. After the laser lift-off process, the sample was dipped into the H_2SO_4

solution to remove the residual Ga on the exposed GaN buffer layers. In the next step, the sample was lapped and polished by diamond powders to smooth the GaN surface since the laser lift-off process left a roughened surface. The mean surface roughness of the polished GaN surface measured by the atomic force microscopy (AFM) is about 1 nm over a scanned area of 20×20 μm^2. However, to prevent the possible damage of the quality in MQWs during the lapping process, the 4-μm GaN bulk layer was preserved. Finally, the second DBR consisting of 8-pair SiO_2/Ta_2O_5 was deposited on the top of the polished GaN surface. The reflectivity of the SiO_2/Ta_2O_5 DBR at 414 nm is 97%. The stopband center of the DBR was also tuned to 450 nm. The thickness of the whole epitaxial cavity was equivalent to the optical thickness of 24.5 emission wavelength. The optical thickness of the MQWs covered nearly half of the emission wavelength right between two adjacent nodes.
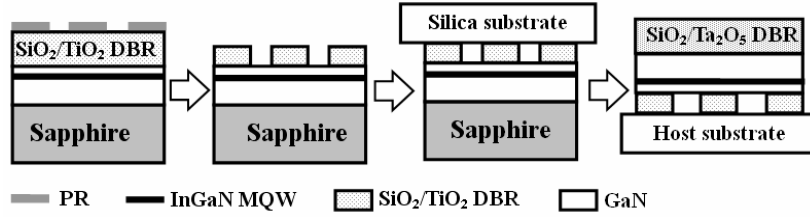

Fig. 7. Schematic process flowchart of the dielectric DBR VCSELs incorporating with two dielectric DBRs fabricated by the later lift-off technique.

Fig. 8 shows the laser emission intensity from the dielectric DBR VCSEL as a function of the pumping energy at room temperature conditions. A clear evidence of threshold condition occurred at the pumping energy of E_{th} = 270 nJ corresponding to an energy density of 21.5 mJ/cm^2. The output laser intensity from the sample increased linearly with the pumping energy level beyond the threshold energy. The estimated carrier density at the threshold is in the order of 10^{20} cm^{-3} assuming that the pumping light with the emission wavelength of 355 nm has experienced a 60% transmission through the SiO_2/Ta_2O_5 DBR layers and undergone a 98% absorption in the thick GaN layer. According to the report by Park [54], the gain coefficient of InGaN at this carrier density level is about 10^4 cm^{-1}. Wang et al. estimated the threshold gain (g_{th}) value of the VCSEL using the equation $g_{th} \geq 1/(\xi L_a) \times \ln(1/R_1R_2)$, where ξ is the axial enhancement factor, L_a is the total thickness of the InGaN MQWs, and R_1 and R_2 are the reflectivity of the dielectric DBRs. Since the active region covers half of the emission wavelength, ξ is unity. They obtained an estimated gain coefficient of about 10^4 cm^{-1} which is consistent with the above g_{th} value estimated from the carrier density. This also proved that the quality of the MQWs had been kept after the laser lift-off and lapping process. The inset shown in Fig. 8 is the laser emission intensity as the function of pumping energy in a logarithmic scale. From the logarithmic data, the spontaneous coupling factor β was estimated from the difference between the heights of the emission intensities before and after the threshold condition. The estimated β was about 1.1×10^{-2}. Since the cavity volume of this dielectric DBR VCSEL is large than the above hybrid DBR VCSEL, the Purcell factor and the spontaneous coupling factor shall be lower accordingly.
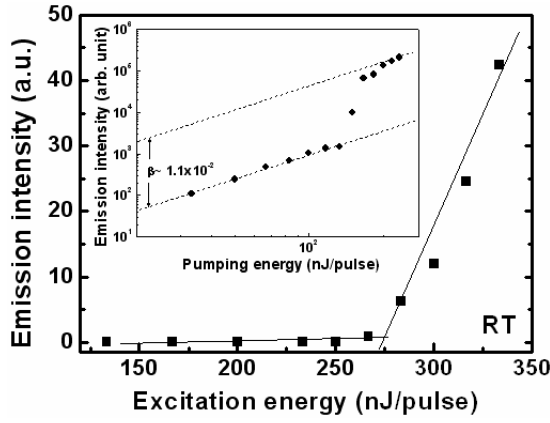
Fig. 8. Laser emission intensity as a function of the exciting energy at room temperature conditions for the dielectric DBR VCSEL. (Inset) Laser emission intensity versus pumping energy in logarithmic scale. The difference between the heights of the emission intensities before and after the threshold corresponds roughly to the value of β. The dash lines are guides for the eye.
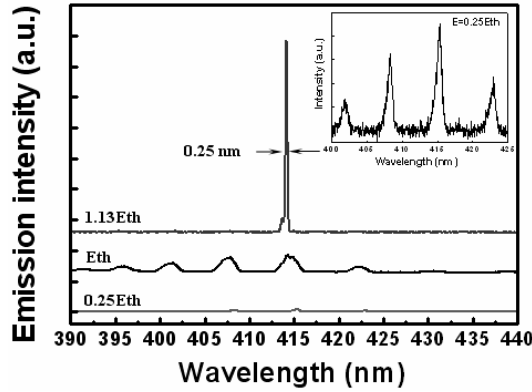

Fig. 9. Emission spectra from the dielectric DBR VCSEL at various pumping energy. The lasing emission wavelength is 414 nm with a linewidth of 0.25 nm. The inset shows the rescaled emission spectrum under pumping power of $0.25E_{th}$.

Fig. 9 shows the evolution of the VCSEL emission spectrum with the pumping energy at room temperature. When the pumping energy is below the threshold, the spontaneous emission spectrum shows multiple cavity modes. The mode spacing is about 7 nm corresponding to a cavity length of 4.3 μm, which is nearly equal to the thickness of the epitaxial cavity. The linewidth of a single cavity mode is 0.8 nm as shown in the inset of Fig. 9. The cavity quality factor estimated from the linewidth is about 518. Considering the optical absorption of GaN layer, an estimated effective cavity reflectivity based on this Q factor is about 97%, which is close to the cavity reflectivity formed by the two dielectric DBRs. This result indicates the laser cavity structure was nearly intact after the laser lift-off process. As the pumping energy increased above the threshold, a dominant laser emission line appeared at 414 nm with a narrow linewidth of about 0.25 nm. The lasing wavelength is located at one of cavity modes near the peak emission wavelength of the InGaN MQWs. The laser emission polarization contrast between two orthogonal directions was measured as well. A degree of polarization of about 70% is estimated. The lower degree of polarization in comparison to the hybrid DBR VCSEL could be due to the smaller Q factor for this dielectric DBR VCSEL.

14

## 1. (b) Research results about electrically pumped GaN-based VCSELs

To fabricate the VCSEL structure for electrical excitation, additional processes for current injection are necessary. Since the epitaxially grown bottom AlN/GaN DBR was un-doped and non-conductive, the epitaxially grown wafer should be further processed to form the intra-cavity co-planar p- and n-contacts for current injection. First, the mesa region was defined by photo-lithography and etched using an inductively coupled plasma reactive ion etching system with Cl_2/Ar as the etching gases to expose the n-GaN layer for the n-contact formation. Then a 0.2-μm thick SiN_x layer was used as the mask to form a current injection and light emitting aperture of 10 μm in diameter, which was then deposited an ITO as the transparent contact layer. Since the ITO locates just next to the VCSEL microcavity, the thickness of 240 nm corresponding to 1λ optical length (λ = 460 nm) has to be accurate to match the phase condition and reduce the microcavity anti-resonance effect. The ITO was annealed at 525°C under the nitrogen ambient to reduce the contact resistance as well as to increase transparency thus reducing the internal cavity loss. A high transmittance of about 98.6% at λ = 460 nm was measured for the deposited ITO after the annealing. Then the metal contact layer was deposited by the electron beam evaporation using Ti/Al/Ni/Au (20/150/20/1000 nm) and Ni/Au (20/1000 nm) as the n-type electrode and p-type electrode to form co-planar intra-cavity contacts, respectively. Finally, an eight-pair Ta_2O_5/SiO_2 dielectric DBR (measured reflectivity of about 99% at λ=460 nm) was deposited on top of the ITO layer to form the top DBR mirror and complete the full hybrid microcavity VCSEL device. Fig. 10(a) shows the schematic of the electrically pumped hybrid GaN-based VCSEL structure. Fig. 10(b) shows the scanning electron microscopy (SEM) image of the completed VCSEL devices. For VCSEL performance characterization, the fabricated VCSEL devices were diced into an individual device size of 120 μm × 150 μm and packaged into the TO-can. The packaged VCSEL device was mounted inside a cryogenic chamber for testing under the 77 K condition. Fig. 10(c) shows the optical microscopy image of a GaN VCSEL sample device at an injection current of 1 mA. The GaN VCSEL sample was placed inside a liquid nitrogen cooled chamber at 77K and tested under CW current injection condition using a CW current source (Keithley 238). The emission light was collected by a 25 μm diameter multimode fiber using a microscope with a 40× objective (numerical aperture = 0.6) and fed into the spectrometer (Triax 320). The system has a focal distance of 320 mm and a grating of 1800 g/mm with a spectral resolution of 0.15 nm. The output from the spectrometer was detected by a charge-coupled device (CCD) to record the emission spectrum. The spatial resolution of the imaging system was about 1 μm as estimated by the diffraction limit of the objective lens. The cross-sectional SEM image of the whole hybrid VCSEL structure is shown in Fig. 11.
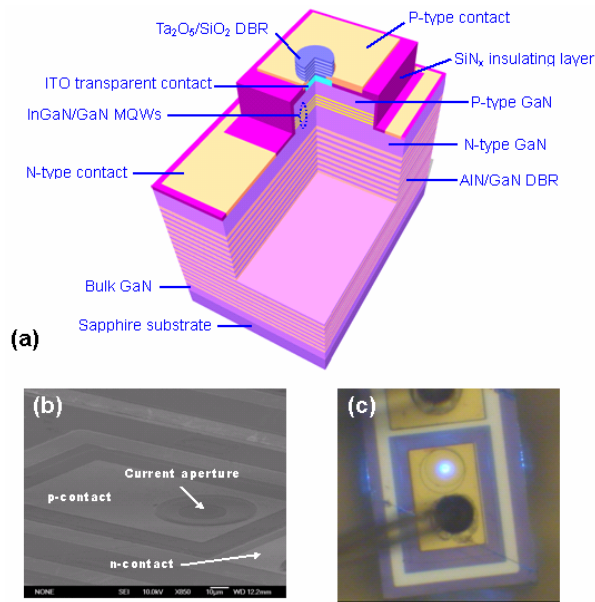
Fig. 10. Structure of electrically pumped hybrid GaN VCSEL. (a) The schematic diagram of the intra-cavity GaN VCSEL. (b) SEM image for the VCSEL with the intra-cavity with two co-planar p- and n-contacts for current injection. (c) The vertical surface emission image of a GaN VCSEL chip at an injection current of 1 mA. The crack line under the p-contact wire bond was occurred during the chipping process.
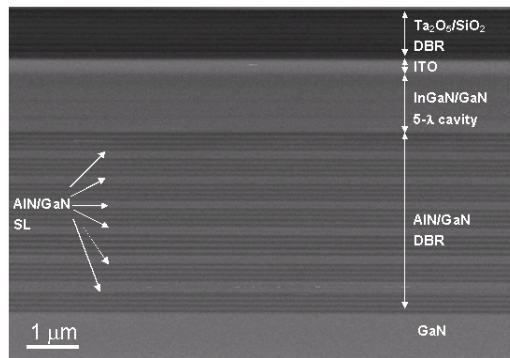
Fig. 11. Cross-sectional SEM image of the whole hybrid GaN-based VCSEL structure with hybrid DBRs, MQWs, and ITO layer.
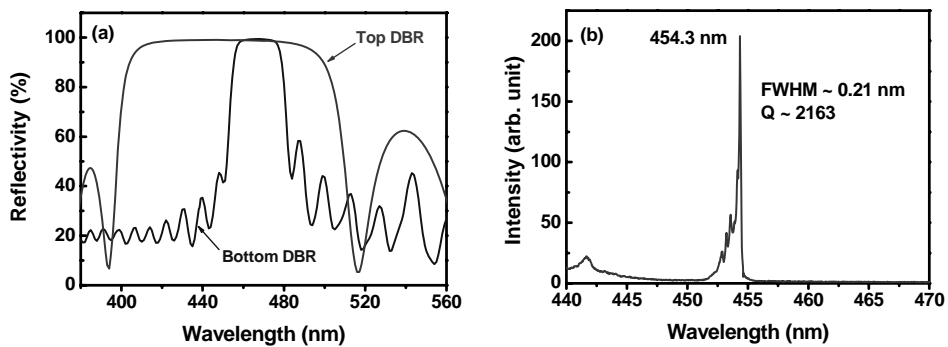
Fig. 12. (a) The reflectivity spectra of top and bottom DBRs show that the highest peak reflectivity of bottom and top DBR is about 99.4% and 99%, respectively. (b) The PL spectrum of the GaN VCSEL structure excited by a CW He-Cd laser (325 nm) at room temperature.

16

Fig. 12(a) shows the reflectivity spectra of crack-free 29-pair AlN/GaN DBR with six SL insertion layers and 8-pair Ta$_2$O$_5$/SiO$_2$ DBR, respectively. A high peak reflectivity of 99.4 % with a spectral band width of ~25 nm was observed from 29-pair AlN/GaN DBR. The flat-topped stopband indicates the high crystal quality of the AlN/GaN DBRs. The 8-pair Ta$_2$O$_5$/SiO$_2$ DBR shows a peak reflectivity of about 99% at 460 nm. The hybrid microcavity quality factor Q of the fabricated GaN VCSEL without the ITO layer was estimated from the PL spectrum of the VCSEL structure as shown in Fig. 12(b). The VCSEL structure was also excited by a CW 325 nm He-Cd laser with a laser spot size of about 1 μm in diameter. From the PL emission peak of 454.3 nm and a narrow linewidth of 0.21 nm, the cavity Q factor can be calculated by $\lambda/\Delta\lambda$ to be about 2200. This Q value is larger than that of the previous optically pumped VCSEL structure, which may originates from the improvement of AlN/GaN DBR reflectivity and the better sample quality. On the other hand, the Q value is slightly higher than the value obtained from the whole VCSEL structure with intra-cavity ITO contact layer due to the additional absorption loss of the ITO.

Fig. 13(a) shows the light output power versus injection current and current-voltage characteristics (typical L-I-V characteristics of a laser) of the VCSEL sample at 77 K. The turn on voltage is about 4.1 V, indicating the good electrical contact of the ITO transparent layer and the intra-cavity structure. The serial resistance of the VCSEL is about 1200 ohm at the driving current of 2.5 mA due to the small current injection aperture. The laser light output power showed a distinct threshold characteristic at the threshold current (I_{th}) of about 1.4 mA then increased linearly with the injection current beyond the threshold. The threshold current density is estimated to be about 1.8 kA/cm^2 for a current injection aperture of 10 μm in diameter. The corresponding threshold carrier density is about 2.6×10^{19} cm^{-3}, estimated by assuming that the carrier lifetime of InGaN MQW is 6.4 ns and the internal quantum efficiency is 0.9 at 77 K [55]. However, according to the observation from CCD image, the injected carriers are not uniformly spreading over the whole 10-μm current aperture, resulting in the spatial non-uniformity in the emission intensity. The actual area for carrier localizations appearing in the current aperture should be much smaller than the 10-μm current aperture. The carrier localization area was estimated to be about 30~50% of the total aperture. Then the carrier density for the lasing spots should be in the range of 5.2×10^{19} to 8.7×10^{19} cm^{-3}. Furthermore, they also estimated the threshold gain coefficient (g_{th}) of the current injection VCSEL operated at 77K using the equation:

$$g_{th} \geq \frac{L_{eff} - d_a}{d_a} <\alpha_i> + \frac{1}{2d_a}\ln\left(\frac{1}{R_1 R_2}\right) \tag{1.3}$$

where L_{eff} is the effective cavity length, $<\alpha_i>$ is the average internal loss inside the cavity, d_a is the total thickness of the multiple quantum well and R_1, R_2 are the reflectivity of the top and bottom DBR mirrors, respectively. Since the internal loss inside the cavity mainly came from the ITO absorption, a threshold gain coefficient value was obstained to be about 8.8×10^3 cm^{-1}, which is a reasonable value for the carrier density in the range of 5.2×10^{19} to 8.7×10^{19} cm^{-3}. Furthermore, the spontaneous emission coupling factor β of the VCSEL sample was estimated from Fig. 13(b), which is the logarithm plot of the Fig. 13(a). The

extracted β value is about 7.5×10^{-2} for the GaN VCSEL. Moreover, the β value was also estimated from the Purcell factor F_p using the approximation equation as that shown in expressions (1) and .2). The cavity Q value is about 1800 based on the emission linewidth of 0.25 nm near the threshold. The optical volume V_c is estimated to be about 1.2×10^{-11} cm^3 for an emission spot size measured to be about 3 μm. The cavity length is about 10.5λ considering the thickness of the ITO and the penetration depth of the DBRs. By using these parameters, a Purcell factor could be estimated to be about 7.9×10^{-2} and an estimated β value of about 7.4×10^{-2} was then obtained. This value is close to that obtained above from Fig. 13(b). The high β value of the microcavity VCSEL could be responsible for low threshold operation of the laser.
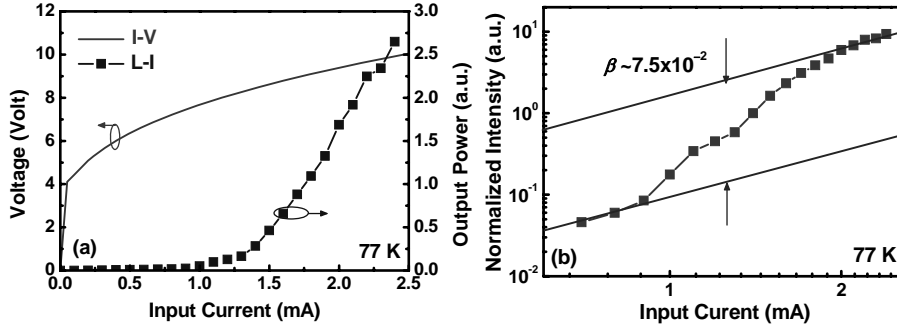
Fig. 13. (a) The light output intensity versus injection current and current-voltage characteristics of GaN VCSEL measured under the CW condition at 77K. (b) The logarithm light output intensity as a function input current at 77 K. The two solid lines are guides for the eye.

Fig. 14 shows the laser emission spectrum at various injection current levels. A dominant single laser emission line at 462.8 nm appears above the threshold current. The inset in Fig. 14 shows the light emission linewidth at various injection current levels. The laser emission spectral linewidth reduces suddenly with the injection current above the threshold current and approaches the spectral resolution limit of 0.15 nm at the injection current of $1.7I_{th}$. Another inset in Fig. 14 shows the CCD image of the spatial laser emission pattern across the 10 μm emission aperture at a slightly below the threshold injection current of 1 mA. The non-uniform emission intensity across the emission aperture with several bright emission spots was observed. Earlier report showed that InGaN MQWs tend to have indium inhomogeneity [56]. Therefore, the non-uniformity in the emission intensity across the aperture could be due to the indium non-uniformity that creates non-uniform spatial gain distribution in the emitting aperture. Actually, the lasing action mainly arises from those spots with brightest intensity as indicated in the inset of Fig. 14. The spatial dimension of these bright spot clusters is only about few μm in diameter. Similar result was also observed and reported recently for the optically pumped GaN VCSELs. The polarization characteristics and far-field pattern (FFP) of the laser emission were also measured. The laser emission has a degree of polarization of about 80% and the FWHM of the FFP is about 11.7° in both horizontal and vertical directions.

18
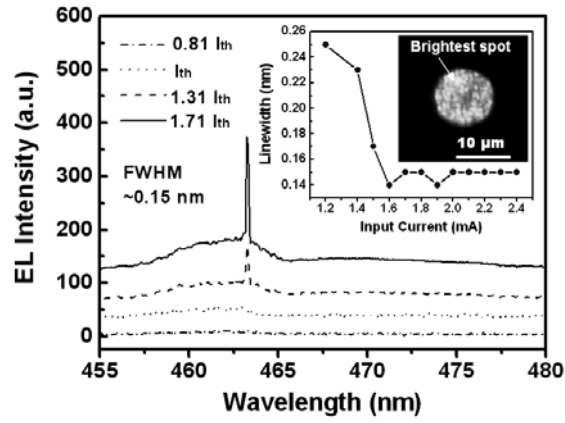
Fig. 14. The laser emission spectrum at different injection current levels measured at 77 K. (Inset) The light emission linewidth at various injection current levels and the CCD image of the emission from the aperture.

## 2. Research results of GaN-based PCSELs

The GaN-based 2D PCSEL was grown by a MOCVD on c-face 2 in diameter sapphire. TMIn, TMGa, TMAl, and ammonia were used as the In, Ga, Al, and N sources, respectively. Fig. 15(a) shows the schematic layer structure of GaN-based 2D PCSELs with bottom AlN/GaN DBRs. The 35 pairs quarter-wave GaN/AlN DBR grown on a 2 μm thick undoped GaN buffer layer was crack free and had a flat surface. Then, an active region grown atop the DBR typically composed of ten $In_{0.2}Ga_{0.8}N$ QWs (L_W=2.5 nm) with GaN barriers (L_B=7.5 nm), and was surrounded by a 560 nm thick Sidoped n-type GaN and a 200 nm thick Mg-doped p-type GaN layer.
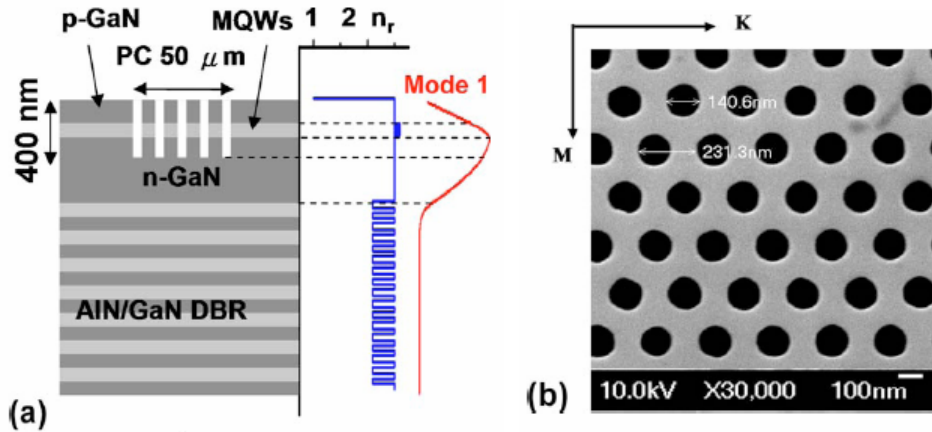
Fig. 15. (a) Schematic layer structure of GaN-based 2D surface-emitting PC lasers with bottom AlN/GaN DBR and the lowest order calculated mode intensity profile along with the refractive index distribution. (b) Top view scanning electron microscope images of the PC structures with hexagonal lattices and circle unit cells.

The typical photoluminescence (PL) spectrum had a peak centered at a wavelength of 425 nm with a linewidth of 25 nm. At normal incidence at RT, the DBR showed the highest reflectivity of 99% at the center wavelength of 430 nm, with a stopband width of about 30 nm, measured by an n&k ultraviolet-visible spectrometer. The as-grown sample was then first deposited with a hard mask consisting of a SiN layer of 200 nm by plasma-enhanced chemical

vapor deposition, followed by a soft mask consisting of a polymethylmethacrylate (PMMA) layer of 150 nm. Using electron-beam lithography, we defined on the soft mask a hexagonal PC pattern with the lattice constant a ranging from 190 to 300 nm and the circular hole diameter r chosen such that r /a is about 0.28. The whole PC pattern is of a circular shape with a diameter of 50 μm. Then, the PC pattern on soft mask was transferred to SiN film by inductively coupled plasma-reactive ion etching (ICP-RIE). After the PMMA layer was removed by acetone, we used ICP-RIE to etch down the as-grown sample to about 400 nm deep. The etching penetrated the QW active regions and created the PC patterns in the nitride layers. Finally, the SiN hard mask was removed by buffered oxide etch dipping. The top view of the hexagonal PC pattern on the GaN-based structure thus created was shown in Fig. 15(b).
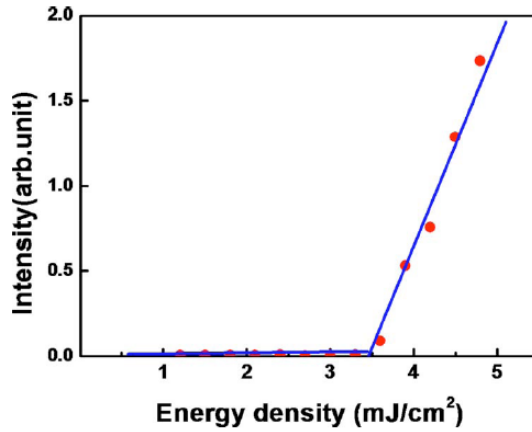
Fig. 16. Measured output intensity versus input excitation energy density from the GaN-based 2D surface-emitting PC lasers with bottom AlN/GaN distributed Bragg reflectors at room temperature.
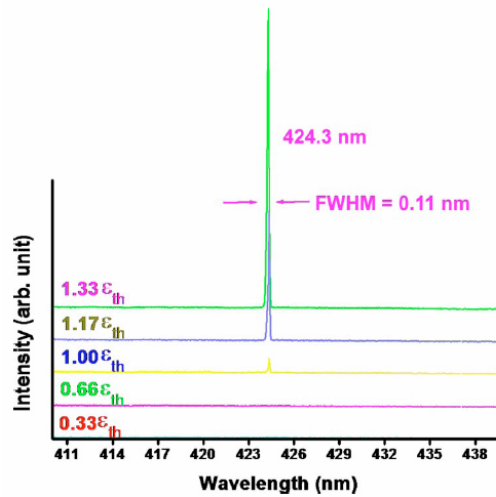
Fig. 17. Emission spectra under varied excitation energy density from the GaN-based 2D surface-emitting PC lasers with bottom AlN/GaN distributed Bragg reflectors at room temperature.

The optical pumping was performed using a frequency tripled Nd:YVO$_4$ 355 nm pulsed laser with a pulse width of ~0.5 ns at a repetition rate of 1 KHz. The pumping laser beam had a spot size of 50 μm and was normally incident onto the sample surface covering the whole PC pattern area. The light emission from the sample was collected by a 15× objective lens through a fiber with a 600 μm core, and coupled into a spectrometer with a charge-coupled device (CCD).

20

The spectral resolution is about 0.1 nm for spectral output measurement. Fig. 16 demonstrates the output emission intensity as a function of the pumping energy density from the sample with PC lattice constant of 290 nm. The clear threshold characteristic was observed at the threshold pumping energy density of 3.5 mJ/cm2, with a peak power density of 7 MW/cm2. Then the laser output increases abruptly with the excitation energy density beyond the threshold. Fig. 17 shows the excitation energy density dependent emission spectra. These spectra clearly show the transition behavior from spontaneous emission to stimulated emission with a single dominant peak. Above the threshold, we can observe only one dominant peak wavelength of 424.3 nm with a full width at half maximum (FWHM) of 0.11 nm limited by our measurement resolution.
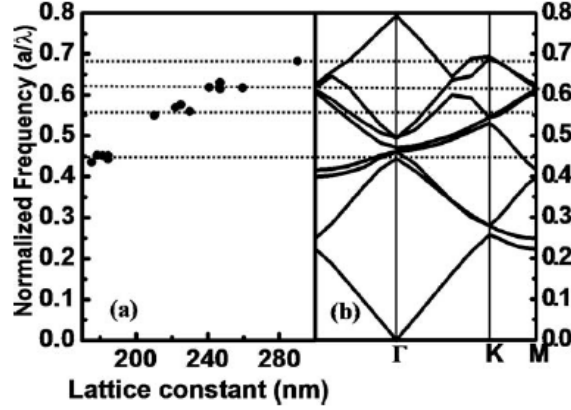
Fig. 18. (a) Normalized frequency as a function of the lattice constant. The solid circle points are the lasing wavelengths from the different PC structures. (b) Calculated band diagram of the 2D hexagonal-lattice structure. The dotted lines are guides for band edges.

It is worth noting that the single mode lasing phenomenon only occurs in the area with PC patterns. On the other hand, multiple lasing peaks were occurred when the area without PC patterns was pumped at the threshold energy density two order of magnitude higher. The normalized frequency (lattice constant over wavelength, a/λ) for the lasing wavelength emitted from our PC lasers with different lattice constants were plotted, as shown in Fig.18(a). All the PC lasers have lasing peaks in a range from 401 to 425 nm. It can be seen that the normalized lasing frequency (dotted points in the figure) increased with the lattice constant in a discontinues and steplike fashion. To calculate the band diagram of the hexagonal PC patterns in this structure, we employ the plane-wave expansion method in two-dimensions with an effective index approach that took into account the effects of partial modal overlap of electromagnetic fields with the PC structures. As a starting point, the ratio of light confined within the 2D PC structure to light extended in the entire device Γ_g and the effective refractive index of the entire device n_{eff} were first estimated by the transfer matrix method. The calculation shows that the lowest order guided mode has the highest confinement factor for both PC and multiple quantum well regions, as shown in Fig. 15(a), and the Γ_g and n_{eff} are estimated to be 0.563 and 2.495, respectively. Then, we determine the effective dielectric constants of the two materials in the unit cell, ε_a and ε_a, using $n_{eff}^2 = f\varepsilon_a+(1-f)\varepsilon_b$ and $\Delta\varepsilon=\varepsilon_b-\varepsilon_a = \Gamma_g(\varepsilon_{mat}-\varepsilon_{air})$, where, the $f=(2\pi r^2/\sqrt{3}\ a^2)$ is a filling factor and ε_{mat} and ε_{air} are dielectric constants of GaN (2.5^2) and air ($=1^2$), respectively. The values of ε_a

(4.11) and ε_b(7.07) thus obtained were then put into the calculation of the band diagram for the 2D hexagonal-lattice structure with r/a =0.28.

Fig. 18(b) shows the calculated band diagram of the 2D hexagonal-lattice structure for transverse-electric mode. It can be expected that the lasing occurs at special points such as at Brillouin-zone boundary near the band edges, because the Bragg condition is satisfied and the density of states is higher in these points. At these lasing points, wave can propagate in different directions and couple with each other. The dotted lines are guides for band edges calculated in Fig. 18(b) and extended horizontally to Fig. 18(a) with the same normalized frequency. It can be seen that different groups of the normalized frequency observed in the PC samples with different lattice constants occur exactly at band edges such as Γ, M, and K points, indicating that the laser operation was provided by multidirectional distributed feedback in the 2D PC structure. The characteristics of Γ, M, and K points lasing can be further identified by the polarization angle of the output emission. Note that the output intensity is higher when some of the lasing frequencies are in the stopband of DBR, which could be due to that the bottom DBR here could be treated as a high reflectivity reflector, facilitating top emission efficiency. The lasing area of the GaN-based 2D surface-emitting PC laser, obtained by a CCD camera is relatively large which covers almost whole area of PC pattern with only one dominant lasing wavelength. The measured FWHM of laser emission divergence angle is smaller than 5°, which is limited by our measurement setup, indicating that the surface emission is almost normal to the PC surface. It's interesting to note that the threshold power density of GaN-based 2D surfaceemitting PC laser is in the same order of or even better than the threshold for GaN-based VCSEL we demonstrated recently. Unlike the small emission spots observed in the GaN-based VCSELs, the large-area emission in 2D surface-emitting PC laser has great potential in applications required high power output operation.

We will further report the characteristics of GaN-based PCSELs and demonstrate the specific lasing characteristics at the following different band edges: Γ, K, and M points calculated by using the plane-wave expansion method. The lasing modes corresponding to the different points of Brillouin-zone boundary can be confirmed by the polarization directions of the laser emissions. Fig. 19(a) shows the laser intensity as a function of the pumping energy at RT condition from the sample with PC lattice constant of 234 nm. The clear evidence of threshold condition occurred at the pumping energy (E_{th}) of 165 nJ corresponding to an energy density of 2.7 mJ/cm2 and the output laser intensity from the sample increased linearly with the pumping energy level beyond the threshold energy. Only one dominated wavelength at 401.8 nm with a linewidth of 1.6 Å was measured, as shown in the inset of Fig. 19(a). Different lasing frequencies were measured from different PC lattice structures. The normalized frequencies as a function of r /a ratio were plotted as square points in Fig. 19(b). On the other hand, we apply the plane-wave expansion method in two dimensions with an effective index model considering the effects of the partial modal overlap of electromagnetic fields with the PC structures to calculate the band diagram of the hexagonal PC patterns in this structure. The solid (black), dot (red), and dash (green) lines are the calculated band edge frequencies at the Γ, K, and M Brillouin-zone

boundaries as a function of r /a ratio, which were in accordance with the measured results.
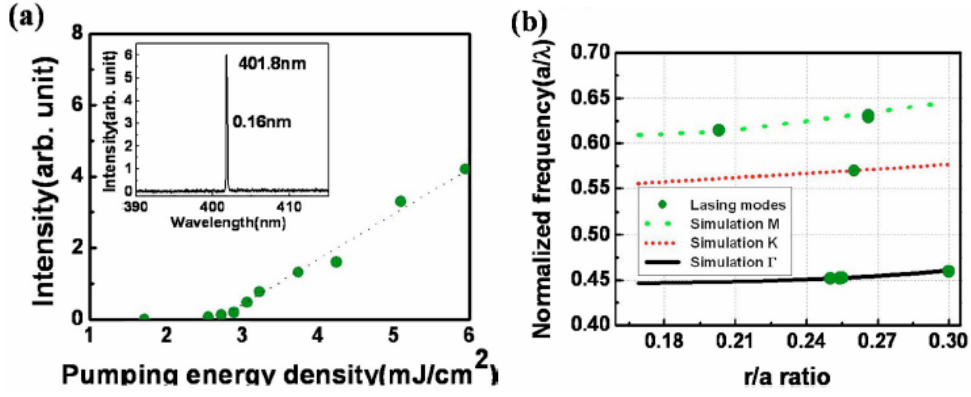

Fig. 19. (a) Laser emission intensity as a function of the pumping energy at room temperature condition for the GaN-based PCSEL. The inset shows only one dominant mode appearing in the lasing spectrum. (b) Normalized frequency vs r /a ratios. The solid (black), dot (red), and dash (green) lines represent the simulation results of Γ, K, and M lasing groups by PWE method. The square points, inserted in the diagram, present the experiment results mapped and compared with the simulation results.
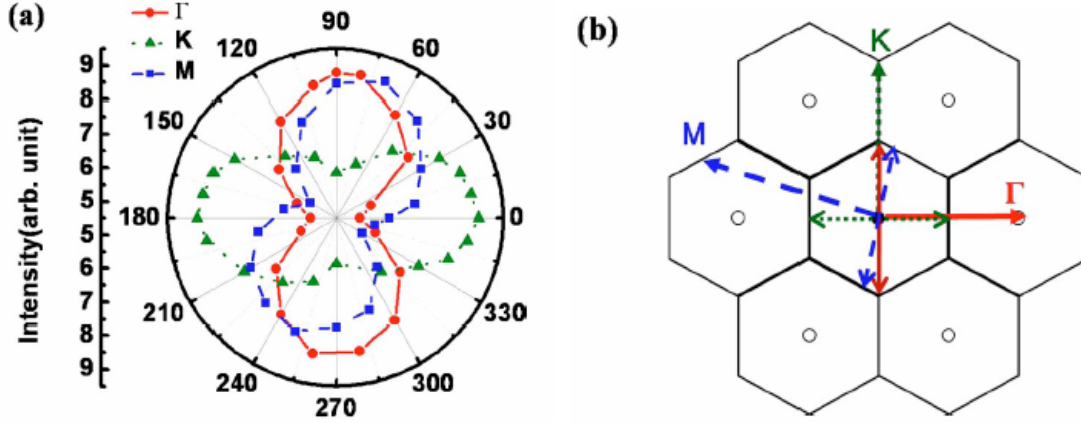
Fig. 20. (a) The measured polarization curves for different band edge lasers grouped into Γ (red-circle points and solid line), K (green triangle points and dot line), and M (blue-square points and dash line) boundaries calculated by the plane-wave expansion method. (b) The main polarization directions obtained in (a) and their corresponding diffracted laser beams, which are normal to the polarization directions in a K-space map corresponding to our hexagonal PC lattice.

The measured polarization curves for different band edge lasers grouped into Γ (red-circle points and solid line), K (green-triangle points and dot line), and M (blue-square points and dash line) boundaries calculated by the planewave expansion method are shown in Fig. 20(a) and the degree of polarization from the emission defined as $(I_{max}-I_{min})/(I_{max}+I_{min})$ was somehow around 50%. The polarization angles from the emissions of devices with different normalized frequencies grouped into Γ, K or M band edge lasers were different. Since the PC lattices provide the optical feedback, which is the origin of the band edge laser operation, the direction and the polarization of the laser light will strictly follow the PC lattice vectors. The symmetric feedback directions provided by the 2D lattice vectors could result in a relatively low degree of polarization if the measurement of the polarization is from the top of the device. As a result, it should be rather

23

difficult to distinguish the specific polarization directions in PCSELs when they are categorized as Γ, K, or M band edge lasers. However, the feedback beams could not be equally diffracted by PC lattices probably due to some disorders or imperfections in the structure. This will result in some beams diffracted in specific directions having higher intensity. The ideally symmetric polarization directions will also be broken. The main polarization directions and the main diffracted laser beams, which are normal to the main polarization directions, can be drawn in a K-space map corresponding to our hexagonal PC lattice, as shown in Fig. 20(b). These main diffracted laser beams, shown as dash lines in Fig. 20(b), point exactly to the Γ (solid-red line), K (dot-green line), and M (dash-blue line) boundaries. The distinct polarization directions provide solid evidence that the lasing actions of our PC laser originate from different band edges.
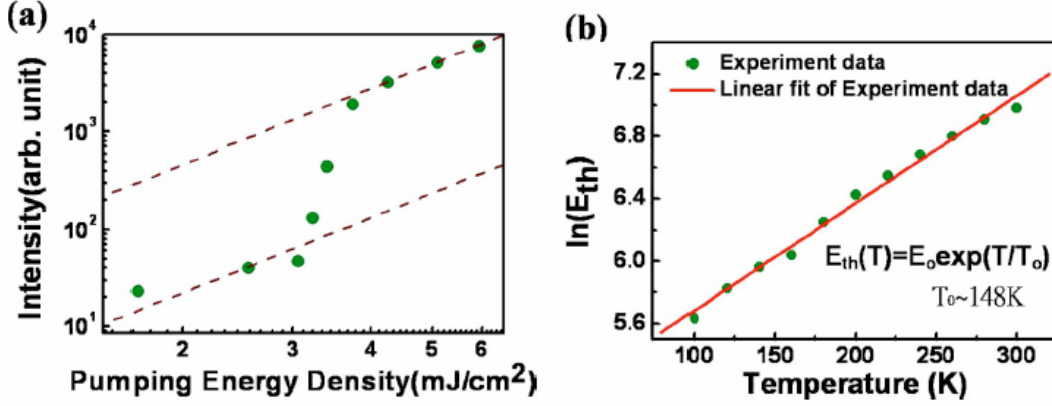

Fig. 21. (a) Laser emission intensity vs pumping energy in a logarithmic scale. The β value estimated from the difference between the two dash lines is about 5×10^{-3}. (b) Temperature dependence of the lasing threshold pumping energy (E_{th}).

To understand the spontaneous coupling factor β of the GaN-based PCSELs, we further replotted the laser emission intensity versed pumping energy from Fig. 19(a) in logarithmic scale, as shown in Fig. 21(a), and then calculated the difference between the heights of the emission intensities before and after the threshold, corresponding roughly to the value of β. The β value of our PCSEL was estimated to be about 5×10^{-3}. Interestingly, this value is smaller than the GaN-based vertical cavity surface emitting lasers. However, the β factor is still larger than the typical edge emitting lasers (normally about 10^{-5}) indicating the enhancement in the spontaneous emission into a lasing mode by the high quality factor in GaN-based PCSELs. Fig. 21(b) shows the seminatural-logarithm plots of the dependence of the threshold pumping energy [In(E_{th})] on the operation temperature (T_0). The threshold energy gradually increased as the operation rose from 100 to 300 K. The relationship between the threshold energy and the operation temperature could be characterized by the equation: $E_{th}=E_0\times e^{T/T0}$, where T_0 is the characteristic temperature and E_0 is a constant. Therefore, we obtain a characteristic temperature of about 148 K by linear fitting of the experiment data, which is close to the value reported for GaN-based edge emitting lasers.

Moreover, we calculated the coupled-wave model in 2-D hexagonal lattice to explain the discrepancy in threshold power with a TE-like mode by considering higher components of Bloch modes and the corresponding coupling coefficients [57], [58]. The single mode lasing phenomenon only occurs in the area with PC patterns. The normalized frequency (lattice constant

over wavelength, a/λ) for the lasing wavelength emitted from our PC lasers with different lattice constants were plotted as shown in Fig. 22(a). All the PC lasers have lasing peaks in a range from 401 nm to 425 nm. It can be seen that the normalized lasing frequency (dotted points in the figure) increased with the lattice constant in a discontinues and step-like fashion. To calculate the band diagram of the hexagonal PC patterns in this structure, we employed the plane-wave expansion method in two-dimensions with an effective index approach that took into account the effects of partial modal overlap of electromagnetic fields with the PC structures [59]. As a starting point, the overlapped ratio of light confined within the 2D PC structure to light extended in the entire device, Γ_g, and the effective refractive index of the entire device n_{eff} were first estimated by using the transfer matrix method. The calculation showed that the lowest order guided mode had the highest confinement factor for both PC and MQW regions and the Γ_g, and n_{eff} were estimated to be 0.563 and 2.495, respectively. Then, we determined the effective dielectric constants of the two materials in the unit cell, ε_a and ε_b, using $n_{eff}^2 = f \cdot \varepsilon_a + (1-f) \cdot \varepsilon_b$ and $\Delta\varepsilon = \varepsilon_b - \varepsilon_a = \Gamma_g \cdot (\varepsilon_{mat} - \varepsilon_{air})$, where $f = 2\pi r^2 /(a^2 \sqrt{3})$ is a filling factor and ε_{mat} and ε_{air} are dielectric constants of GaN (= 2.5^2) and air (= 1^2), respectively. The values of ε_a (4.11) and ε_b (7.07) thus obtained were then put into the calculation of the band diagram for the 2D hexagonal-lattice structure with $r/a = 0.25$.
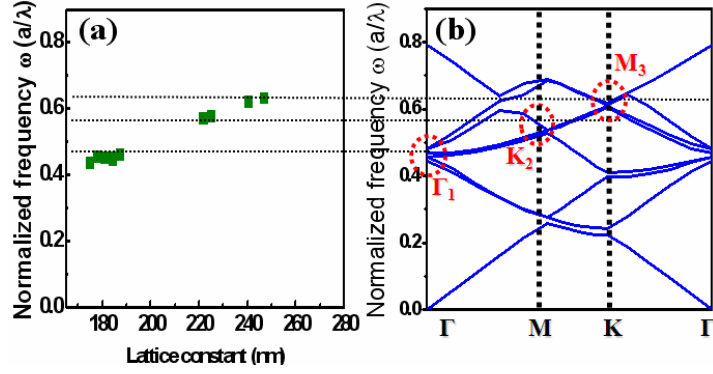
Fig. 22. (a) Normalized frequency verses PC lattice constant. The solid square points are the lasing wavelengths from the different PC structures. (b) Calculated band diagram of the 2D hexagonal-lattice structure. The dotted lines are guides for band edges.

Fig. 22(b) shows the calculated band diagram of the 2D hexagonal-lattice structure for transverse-electric (TE) mode. It can be expected that the lasing occurs at special points such as at Brillouin-zone boundary near the band edges, because the Bragg condition is satisfied and the density of states is higher at these band edges [59]. At these lasing points, wave can propagate in different directions and couple with each other. The dotted lines are guides for band edges calculated in Fig. 22(b) and extended horizontally to Fig. 22(a) with the same normalized frequency. It can be seen that different groups of the normalized frequency observed in the PC samples with different lattice constants occur exactly at band edges such as Γ, M, and K points (or more specifically labeled as Γ1, K2, M3), indicating that the laser operation was provided by multidirectional distributed feedback in the 2D PC structure [60]. The characteristics of Γ, M, and K points lasing can be further identified by the polarization angle of the output emission. Note that the output intensity is higher when some of the lasing frequencies are in the stopband of DBR, which could be due to that the bottom DBR here can be treated as a high reflectivity reflector, facilitating top-emission efficiency. As shown in Fig. 23, we are able to classify the

lasing actions into three groups, where lasing within Γ1 mode shows the lowest threshold power while lasing within M3 mode has the highest threshold power. Such results could be attributed to the different coupling effects at different band edges, which can be explained by coupled-wave model calculation.
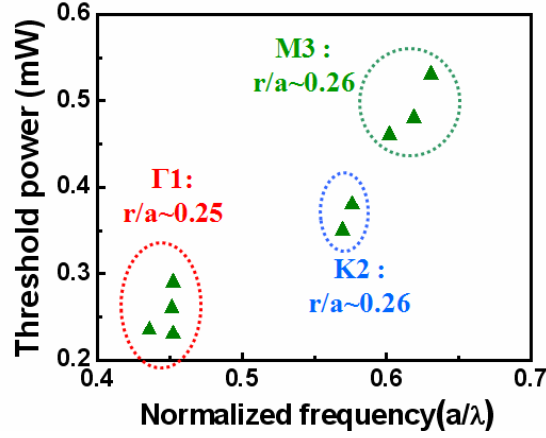
Fig. 23. Different threshold power versus normalized frequency.
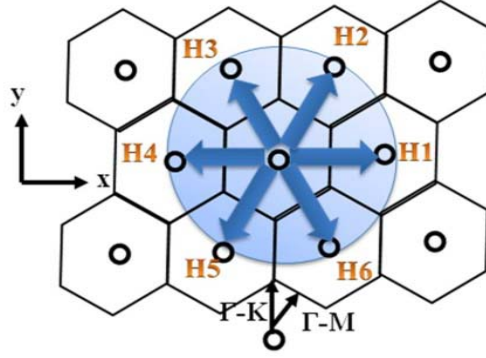
Fig. 24. Schematic diagram of six propagation waves in hexagonal lattice for Γ1 band.

To simplify the calculation, the 2D PC structure investigated here consists of an infinite hexagonal lattice with circular air holes in the *x* and *y* directions. The corresponding 2D K space is shown in Fig. 24. The structure is also assumed to be uniform in the *z* direction. In addition, the gain effects are neglected here during the calculation to extract the pure diffraction effects. While considering the infinite structure, the scalar wave equation for the magnetic field H_z in the TE mode can be written as

$$\frac{\partial^2 H_z}{\partial x^2} + \frac{\partial^2 H_z}{\partial y^2} + k^2 H_z = 0, \tag{2.1}$$

where

$$k^2 = \beta^2 + 2j\alpha\beta + 2\beta\sum_{G\neq 0} k(G)\exp\left[j(G\cdot r)\right], \tag{2.2}$$

And the magnetic field can be described by the Bloch mode when considering the Γ1 band edge as shown in Fig. 24:

26

$$H_z(r) = \sum_G h_G \exp\left[j(k+G) \cdot r\right],\tag{2.3}$$

where

$$H_z = H_1(x,y)e^{-i\beta_0\hat{x}} + H_2 e^{-i\beta_0(\frac{1}{2}\hat{x}+\frac{\sqrt{3}}{2}\hat{y})} + H_3 e^{-i\beta_0(\frac{-1}{2}\hat{x}+\frac{\sqrt{3}}{2}\hat{y})}$$

$$+H_4 e^{i\beta_0\hat{x}} + H_5 e^{-i\beta_0(\frac{-1}{2}\hat{x}-\frac{\sqrt{3}}{2}\hat{y})} + H_6 e^{-i\beta_0(\frac{1}{2}\hat{x}-\frac{\sqrt{3}}{2}\hat{y})},\tag{2.4}$$

Substituting Eq. (2.4) and Eq. (2.2) into Eq. (2.1), and comparing the equal exponential terms, we can obtain six wave equations.

$$-\frac{\partial}{\partial x}H_1 + (-\alpha - i\delta)H_1 = -i\frac{\kappa_1}{2}(H_2+H_6) + i\frac{\kappa_2}{2}(H_3+H_5) + i\kappa_3 H_4$$

$$-\frac{1}{2}\frac{\partial}{\partial x}H_2 - \frac{\sqrt{3}}{2}\frac{\partial}{\partial y}H_2 + (-\alpha - i\delta)H_2 = -i\frac{\kappa_1}{2}(H_1+H_3) + i\frac{\kappa_2}{2}(H_4+H_6) + i\kappa_3 H_5$$

$$-\frac{1}{2}\frac{\partial}{\partial x}H_3 - \frac{\sqrt{3}}{2}\frac{\partial}{\partial y}H_3 + (-\alpha - i\delta)H_3 = -i\frac{\kappa_1}{2}(H_2+H_4) + i\frac{\kappa_2}{2}(H_1+H_5) + i\kappa_3 H_6$$

$$\frac{\partial}{\partial x}H_4 + (-\alpha - i\delta)H_4 = -i\frac{\kappa_1}{2}(H_3+H_5) + i\frac{\kappa_2}{2}(H_2+H_6) + i\kappa_3 H_1$$

$$\frac{1}{2}\frac{\partial}{\partial x}H_5 + \frac{\sqrt{3}}{2}\frac{\partial}{\partial y}H_5 + (-\alpha - i\delta)H_5 = -i\frac{\kappa_1}{2}(H_4+H_6) + i\frac{\kappa_2}{2}(H_1+H_3) + i\kappa_3 H_2$$

$$-\frac{1}{2}\frac{\partial}{\partial x}H_6 + \frac{\sqrt{3}}{2}\frac{\partial}{\partial y}H_6 + (-\alpha - i\delta)H_6 = -i\frac{\kappa_1}{2}(H_1+H_5) + i\frac{\kappa_2}{2}(H_2+H_4) + i\kappa_3 H_3$$

$$\text{(2.5.a-e)}$$

where H_1, H_2, H_3, H_4, H_5 and H_6 express the envelope magnetic field distributions of individual light waves propagating in the six equivalent Γ-M directions: 0°, +60°, +120°,+180°, +240°, and +300° with respect to the x-axis. κ_1, κ_2, and κ_3 are the coupling coefficients between light waves propagating at 60° to each other (H_1 and H_2, H_2 and H_3, and so on), at 120° (H_1 and H_3, H_2 and H_4, and so on), and at 180° (H_1 and H_4, H_2 and H_5, and so on), respectively. δ is the deviation of the wave number β (expressed as $2\pi v/c$, where v is the frequency and c is the velocity of light) from the fundamental propagation constant β_0 (equal to $4\pi/\sqrt{3}a$, where a is the lattice constant) for each cavity mode, and expressed as $\delta = (\beta^2 - \beta_0^2)/2\beta_0$. α is the corresponding threshold gain.

By solving Eq. (2.5.a-e), an eigen frequency v for each band-edge mode and the corresponding threshold gain α for a given set of coupling coefficients, κ_1, κ_2, and κ_3, can be obtained. When only the eigen frequencies are concerned, the derivation terms and the threshold gain α in Eq. (2.5.a-e) can be set to zero, and the individual eigen frequencies can then be derived as follows:

$$v_1 = \frac{c}{2\pi n_{eff}}(\beta_0 - \kappa_1 - \kappa_2 + \kappa_3)\tag{2.6.a}$$

$$v_2 = \frac{c}{2\pi n_{eff}}(\beta_0 - \frac{1}{2}\kappa_1 + \frac{1}{2}\kappa_2 - \kappa_3) \tag{2.6.b}$$

$$v_3 = \frac{c}{2\pi n_{eff}}(\beta_0 + \kappa_1 - \kappa_2 - \kappa_3) \tag{2.6.c}$$

$$v_4 = \frac{c}{2\pi n_{eff}}(\beta_0 + \frac{1}{2}\kappa_1 + \frac{1}{2}\kappa_2 + \kappa_3) \tag{2.6.d}$$

where, c is the velocity of a photon in vacuum, and n_{eff} is the effective refractive index of the device structure. There are four eigen mode frequencies, v_1 to v_4, which correspond to the four band-edges, including two degenerate modes with v_2 and v_4. Once the frequency of the eigen mode at the individual band-edges is obtained, the coupling coefficients κ_1, κ_2, and κ_3, can be derived from Eq. (2.6.a-d) as follows:

$$\kappa_1 = \frac{-v_1 - v_2 + v_3 + v_4}{v_1 + 2v_2 + v_3 + 2v_4}2\beta_0 \tag{2.7.a}$$

$$\kappa_2 = \frac{-v_1 + v_2 - v_3 + v_4}{v_1 + 2v_2 + v_3 + 2v_4}2\beta_0 \tag{2.7.b}$$

$$\kappa_3 = \frac{v_1 - 2v_2 - v_3 + 2v_4}{v_1 + 2v_2 + v_3 + 2v_4}2\beta_0 \tag{2.7.c}$$

By comparing the value of coupling coefficients κ_1, κ_2, and κ_3, based on actual device parameters, we can determine which kind of distributed feedback mechanism provide the major significant contribution to support the lasing oscillation at Γ1 band edge.
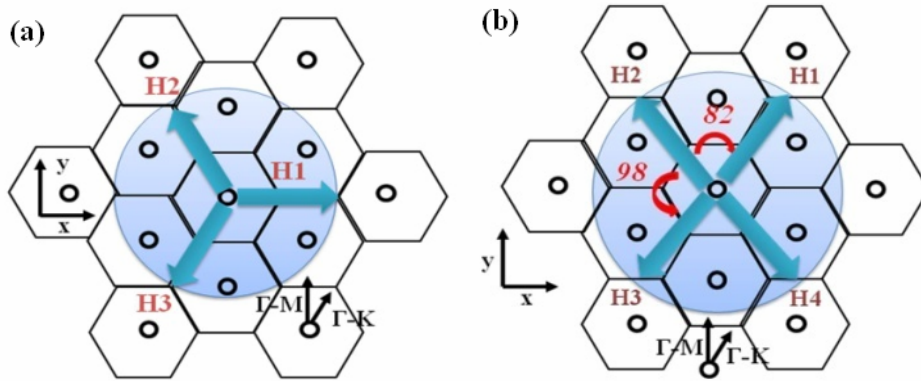
Fig. 25. Schematic diagram of propagation waves in hexagonal lattice for (a) K2 band edge; (b) M3 band edge.

Similarly, we use the same calculation method to solve coupling coefficients for K2 and M3 operation modes. We can obtain two individual eigen mode frequencies for K2 and four eigen mode frequencies for M3, listed as below:

(1) K2 (shown in Fig. 25(a). There are two eigen mode frequencies with only one coupling angle at 120° for one coupling coefficient.)

$$\kappa = \frac{v_2 - v_1}{v_1 + 2v_2} 2\beta_0 \qquad (2.8)$$

(2) M3 (shown Fig. 25(b). There are four eigen mode frequencies with three coupling angles, i.e. 82°, 98°, and 180° for coupling coefficients κ_1, κ_2, and κ_3.)

$$\kappa_1 = \frac{v_1 - v_2 - v_3 + v_4}{v_1 + v_2 + v_3 + v_4} \beta_0 \qquad (2.9.a)$$

$$\kappa_2 = \frac{-v_1 + v_2 - v_3 + v_4}{v_1 + v_2 + v_3 + v_4} \beta_0 \qquad (2.9.b)$$

$$\kappa_3 = \frac{-v_1 - v_2 + v_3 + v_4}{v_1 + v_2 + v_3 + v_4} \beta_0 \qquad (2.9.c)$$

The coupling coefficient of each PC surface-emitting laser could be then evaluated by using the band edge frequencies shown in Fig. 22(b). First, for $\Gamma 1$ mode, substituting the normalized frequencies, 0.4482, 0.4595, 0.4704, 0.4930 with the PC lattice constant of about 180 nm into the expression of Eq 2.7(a), 2.7(b), and 2.7(c), we obtain the coupling coefficients $\kappa_1 \sim 17480$, $\kappa_2 \sim 11240$, $\kappa_3 \sim 11268$ (cm^{-1}). The largest coupling coefficient κ_1 shows that the light waves propagating at 60° to each other dominate the coupling effect. Similarly, for K2 mode, substituting the normalized frequencies 0.5326 and 0.5413 with the PC lattice constant of about 220 nm into the expression of Eq 2.8, we obtained the coupling coefficient $\kappa \sim 4089$ (cm^{-1}).

For M3 mode, substituting the normalized frequencies, 0.6089, 0.6094, 0.6141, and 0.6234 with the PC lattice constant of about 247 nm into the expression of Eq 2.9(a), 2.9(b), and 2.9(c), we obtain the coupling coefficient $\kappa_1 \sim 1241$, $\kappa_2 \sim 1356$, $\kappa_3 \sim 2683$ (cm^{-1}). The largest coupling coefficient κ_3 shows that greatest feedback effect is similar to that of a conventional in-plane distributed feedback laser. Moreover, it is interesting to note that the lasing action within $\Gamma 1$ mode shows the lowest threshold power in Fig. 23, which could be attributed to the largest coupling coefficient. On the other hand, lasing within M3 mode has the highest threshold power due to the lowest coupling coefficient.

3. Semiconductor microcavity polaritons

In order to study the optical properties of ZnO-based MC polaritons, growth of high-quality ZnO films and fabrication of high-Q ZnO MCs are necessary. Furthermore, the knowledge of the polariton dispersion curves from ZnO-based MCs at RT is crucial for the advanced design of polariton-based optoelectronic devices operating at high working temperature. In this study, we report the experimental observation of strong coupling regime in bulk ZnO-based hybrid MCs at RT according to the angle-resolved reflectivity spectra. The investigated structure consists of a $3\lambda/2$ bulk ZnO cavity layer sandwiched between two high-reflectivity DBRs and has a cavity quality factor (Q) about 250, which is the state of the art for a ZnO-based MC. Furthermore, the measured angle-resolved reflectivity spectra are theoretically investigated by employing transfer matrix method and the influence of exciton scattering states is also taken into account in our

calculations to compare the experimental and theoretical results.

The present hybrid MC structure consists of a bulk ZnO $3\lambda/2$ thick cavity sandwiched between a bottom 30-pair AlN/$Al_{0.23}Ga_{0.77}$N DBR and a top 9-pair dielectric SiO_2/HfO_2 DBR. The AlN/AlGaN DBR was grown by metalorganic chemical vapor deposition (MOCVD) on a 3 μm thick GaN buffer layer on c-plane sapphire substrate. During the growth, TMGa and TMAl were used as group III source materials and NH_3 as the group V source material. After thermal cleaning of the substrate in hydrogen ambient for 5 min at 1100 °C, a 30-nm-thick GaN nucleation layer was grown at 520 °C. The growth temperature was raised up to 1040 °C for the growth of 3 μm GaN buffer layer. Then, the AlN/AlGaN DBRs were grown under the fixed chamber pressure of 100 Torr. The bulk ZnO $3\lambda/2$ thick cavity was grown on AlN/AlGaN DBR by pulsed-laser deposition (PLD) system, which is commonly adopted for the growth of ZnO epi-films [61]. The beam of a KrF excimer laser ($\lambda = 248$ nm) was focused to produce an energy density ~5–7 J·cm^{-2} at a repetition rate 10 Hz on a commercial hot-pressed stoichiometric ZnO (99.999 % purity) target. The ZnO films were deposited with a growth rate ~0.5475 Å s^{-1} at substrate temperature of 600 °C and a working pressure ~ 9.8×10^{-8} Torr without oxygen gas flow. Finally, the 9-period SiO_2/HfO_2 dielectric DBR was deposited by dual electron-beam gun evaporation system to complete the MC structure. The low-magnification cross-section SEM image of the ZnO hybrid MC structure is shown in Fig. 26(a). Fig. 26(b) shows the cross-section SEM image of the AlGaN/AlN and SiO_2/HfO_2 DBRs, and ZnO bulk layer under high magnification. The interfaces between each layer are well defined. To further illustrate the configuration of the hybrid MC structure, the refractive index profile and the electric-field intensity in the growth direction for normal incidence at photon energy of 3.23 eV are displayed in Fig. 27.
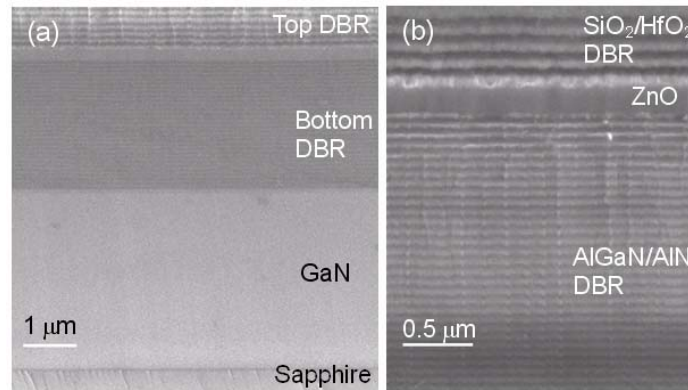
Fig. 26. (a) Low-magnification cross-section scanning electron microscopy image of the $3\lambda/2$ bulk ZnO hybrid microcavity structure. (b) Cross-section scanning electron microscopy image of the AlGaN/AlN and SiO_2/HfO_2 DBRs, and the $3\lambda/2$ ZnO bulk layer under high magnification.

RT microphotoluminescence (μPL) spectra were performed under normal incidence by focusing the laser beam using an UV microscope objective (15×) which makes the laser spot size about 3 μm. The emission light from sample surface was collected along the normal direction by a 600 μm core UV optical fiber. The excitation source of the PL measurements is a 266 nm radiation from a frequency tripled Ti:sapphire laser. RT angle-resolved reflectivity measurements

were carried out by using a two arm goniometer and a xenon lamp was employed as a white light source combined with a 100 μm core optical fiber. The reflected light was then collected by a 600 μm core UV optical fiber mounted on a rotating stage with an angular resolution of ~1° and detected by a liquid nitrogen cooled charge-coupled device (CCD) attached to a 320 mm single monochromator with a spectral resolution of about 0.2 nm.
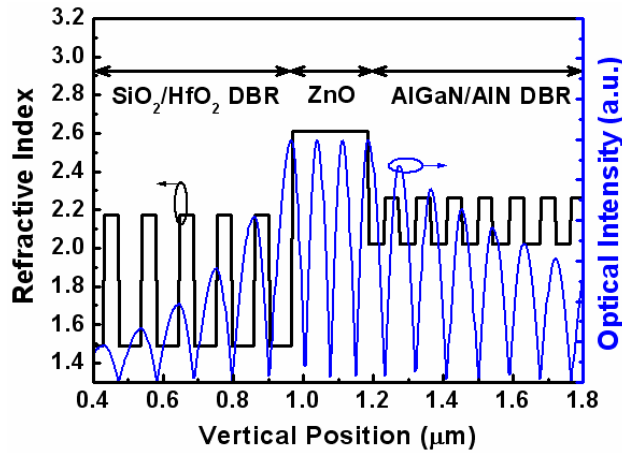
Fig. 27. Refractive index profile and the electric-field intensity in the growth direction for normal incidence at photon energy of 3.23 eV.

Fig. 28. Refractive index profile and the electric-field intensity in the growth direction for normal incidence at photon energy of 3.23 eV.

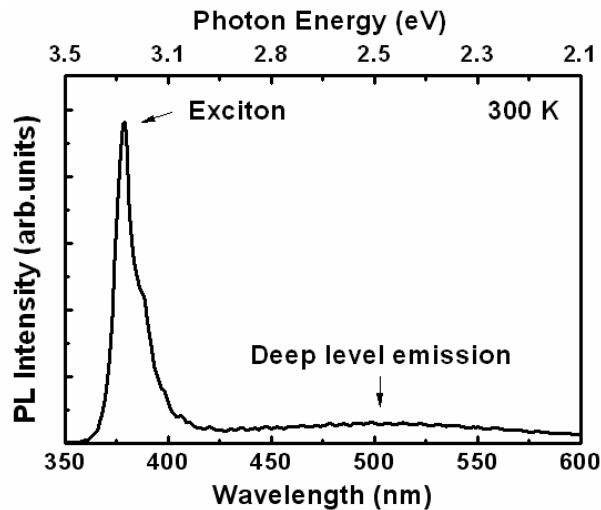The optical properties of the 3λ/2 ZnO film grown on 30-pair AlN/AlGaN DBR were investigated by performing the RT PL measurements, as shown in Fig. 28. The half-cavity structure exhibited strong near-band-edge emission around 378 nm (3.28 eV), which has been known to be of free excitonic nature [62]. Additionally, the green PL mainly comes from the deep-level emission which is related to the crystal defects, such as oxygen vacancies and zinc interstitials in the films as reported by Vanheusden *et al.* [63]. The good material quality of the ZnO film can be observed from the suppression of the deep level emission band in the RT PL spectrum. Another feature of the PL spectrum is the long tail extending from the near-band-edge emission. This property is usually observed from RT PL spectra of ZnO films and caused by band structure deformation due to the crystal lattice deformation [64]. Moreover, it is noteworthy that

the growth of 3λ/2 cavity length, which is relatively thicker than λ/2 or λ cavity is employed in this study since the ZnO crystal quality and optical properties can be effectively improved by increasing the film thickness [65].
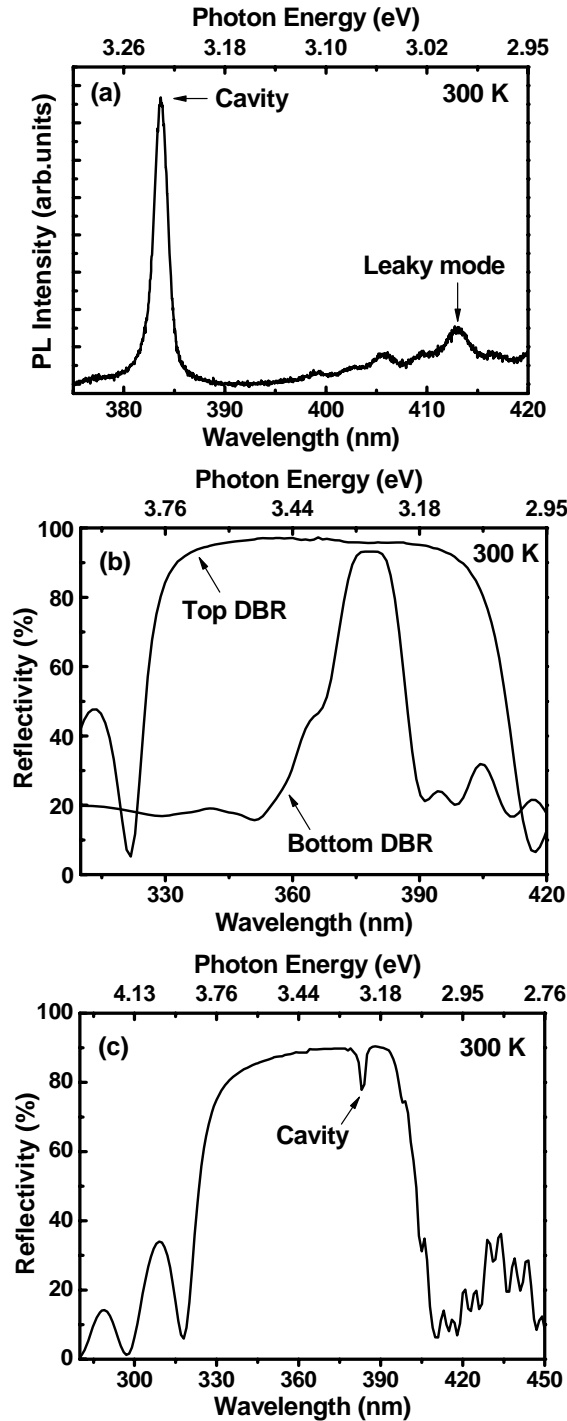
Fig. 29. (a) RT normal incidence μPL spectrum of the full ZnO hybrid microcavity structure. The emission peak energy is nearly pure cavity photon mode because of the large negative exciton-photon detuning. (b) The RT reflectivity spectra of a 30-pair AlN/Al$_{0.23}$Ga$_{0.77}$N DBR (dashed line) and a 9-pair SiO$_2$/HfO$_2$ DBR (solid line). (c) RT normal incidence reflectivity spectrum of the full ZnO microcavity structure.

In order to investigate the optical quality of the full ZnO MC structure, the RT μPL measurements were performed at normal incidence and the corresponding PL spectrum is shown in Fig. 29(a). The emission peak energy of the full ZnO MC is about 3.232 eV ($\lambda \sim 383.6$ nm), which means that the emission peak is nearly a pure cavity photon mode because of the large

negative detuning between cavity photon energy at zero in-plane wave vector and exciton energy ($\Delta = E_{ph} - E_{ex}$). Under this circumstance, we can estimate the intrinsic cavity quality factor with the minimum perturbation of the exciton-photon coupling. From Fig. 29(a), the PL linewidh is only 13 meV ($\Delta\lambda \sim 1.53$ nm) due to the MC effect. Therefore, the cavity quality factor Q ($=\lambda/\Delta\lambda$) is about 250 based on the μPL measurement results. Such a Q value is the state of the art for ZnO-based MCs and demonstrates the high local quality of our ZnO MC structures. Moreover, another relatively week PL emission peak was observed at 413 nm in Fig. 29(a). This emission originates from the Bragg leaky modes of the top SiO_2/HfO_2 DBR structure. The reflectivity spectra of the 30-pair $AlN/Al_{0.23}Ga_{0.77}N$ DBR and the 9-pair SiO_2/HfO_2 DBR were measured at RT respectively for normal incidence, as shown in Fig. 29(b). The peak reflectivity of bottom AlN/AlGaN DBR is about 93% and the stop band width is about 145 meV. As for the top SiO_2/HfO_2 DBR, the peak reflectivity and the stop band width are 97% and 790 meV, respectively. Fig. 29(c) shows the RT normal incidence reflectivity spectrum of the full ZnO MC structure. The cavity dip can be clearly observed in the reflectivity spectrum, which shows a precise alignment between the DBR stop band and the ZnO cavity thickness. Although the measurement of the reflectivity spectrum was performed by using an optical lens to focus the incident while light beam, which results in a relatively larger spot size, the cavity dip (~ 383.4 nm) is consistent with the μPL measurement results. Nevertheless, the microscopic fluctuation in thickness, interface roughness, and crystal imperfection will cause the inhomogeneous broadening of the cavity mode when we use the incident while light beam with a larger spot size ($\sim$50 μm in diameter). As a result, a relatively lower Q factor ~ 196 was extracted from the reflectivity spectrum shown in Fig. 29(c) as compared with that from the μPL measurement. Furthermore, the irregular long wavelength oscillations of the reflectivity spectrum arise from the modulation of the respective top and bottom DBR spectra. On the contrary, the short wavelength oscillator is relatively regular, which only results from the top dielectric DBR since the short-wavelength light is absorbed by AlGaN layers in the bottom nitride-based DBR structure.

To further probe the characteristics of strong exciton-photon coupling in the ZnO MC structure, RT angle-resolved reflectivity measurements were performed for the observation of in-plane polariton dispersion curves. The color map of the angular dispersion of measured reflectivity spectra from 8 to 38° is shown in Fig. 30(a). Furthermore, the color maps of the calculated angle-resolved reflectivity spectra without and with taking the resonant exciton into account are shown in Figs. 30(b) and 30(c), respectively. The dashed white lines represent the calculated dispersion curves including exciton mode, cavity mode, lower polariton branch (LPB), and upper polariton branch (UPB). In our simulation, the reflectivity spectra were carried out based on transfer matrix method and the resonant exciton was modeled by a Lorentz oscillator dispersive dielectric function, which can be expressed as follows:

$$\varepsilon_r(E) = \varepsilon_b + \frac{B}{E_0^2 - E^2 + j\Gamma E}, \tag{3.1}$$

where E_0 is the exciton transition energy. The physical parameter B is related to the exciton oscillator strength and Γ is the broadening parameter. Originally, the planar cavity photon

dispersion with small in-plane wave vector $k_{//}$ can be expressed as

$$E_{ph}(k_{//}) = \frac{\hbar c}{n}\sqrt{\left(\frac{2\pi}{L}\right)^2 + k_{//}^2} \approx \frac{2\pi\hbar c}{nL} + \frac{\hbar c L}{4\pi n}k_{//}^2, \tag{3.2}$$

where n is the effective cavity refractive index and L is the effective cavity length. Therefore, the pure in-plane cavity dispersion will take this parabolic form. Nevertheless, the in-plane dispersion of polaritons depends on the dispersion of photons and the degree of the mixing with excitons. By comparing Figs. 30(a) and 30(b), the pure cavity mode follows the parabolic dispersion, which is consistent with the Bragg mode (BM) from the low energy side of the stop band. Nevertheless, the measured dispersion of the LPB obviously deviates from the parabolic cavity mode and approaches to exciton mode with increasing angle.
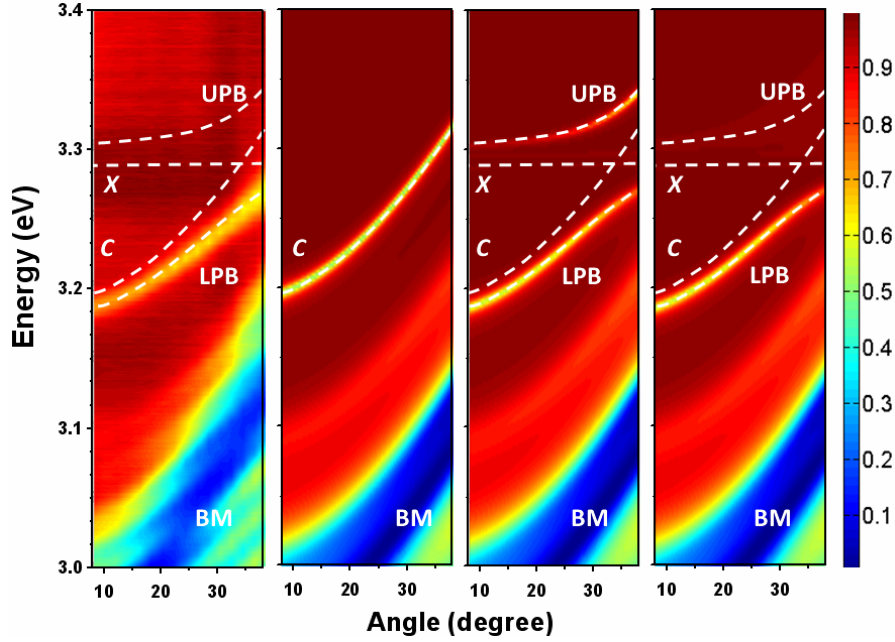
Fig. 30. (a) Color map of the angular dispersion of measured reflectivity spectra from 8 to 38° at RT. (b) Color maps of the calculated angle-resolved reflectivity spectra without taking the resonant exciton into account. (c) Color maps of the calculated angle-resolved reflectivity spectra with taking the resonant exciton into account. (d) Simulation of angle-resolved reflectivity spectra for the bulk ZnO MCs after taking the absorption continuum into account.

Furthermore, a good agreement is found between the experimental and theoretical LPBs, as shown in Figs. 30(a) and 30(c), when we consider the strong exciton-photon coupling in our calculation by assigning the parameter B related to the oscillator strength of about 10^5 meV^2. This value is nearly two times more than that of GaN-based materials due to the larger oscillator strength of ZnO materials. In addition, this value is also in good agreement with the recently published value. As can be seen from Fig. 30(c), we estimated that the anticrossing occurs near the angle of about 34° and the corresponding vacuum Rabi splitting value is about 72 meV. This large vacuum Rabi splitting is a state-of-the-art value in ZnO MCs at RT, which may originate from the high cavity quality factor, good ZnO crystal quality, and larger ZnO thickness. On the other hand, although the angular dispersion of the LPB is well visible from experimental results, the signature of the UPB is not observable, as shown in Fig. 30(a). Moreover, another interesting issue regarding the anticrossing behavior in bulk ZnO MCs was investigated by Faure *et al.* in

2008. They theoretically expected that the anticrossing behavior can be properly defined in bulk GaAs and GaN MCs (i.e., the upper and lower polariton branches can be probed by experimental measurements), whereas only the lower polariton branch (LPB) is a well-defined and well-mixed exciton-photon state in bulk ZnO MCs. They proposed that the upper polariton branch (UPB) in bulk ZnO MCs is strongly damped due to the absorption by scattering states of excitons.

In order to understand the invisible UPB in bulk ZnO MCs, we further take into account the effect of absorption continuum induced by scattering states of the exciton in our simulation. The absorption continuum is added to the dielectric function and the amplitude is adjusted to match the experimental absorption spectra [66]. Fig. 30(d) presents the simulation of angle-resolved reflectivity spectra for the bulk ZnO MCs after taking the absorption continuum into account. It is clearly observed that the UPB is significantly broadened due to its crossing with the continuum states of excitons. In wide bandgap semiconductor-based MCs, the vacuum Rabi splitting energy is nearly the same or larger than the exciton binding energies, especially for ZnO-based MCs, which will give rise to the energy overlap between the UPB and the continuum states. Such a situation is especially important for bulk ZnO MCs due to the relatively thick cavity layer and the large absorption coefficient ($\sim 2 \times 10^5$ cm^{-1}) for ZnO materials [67]. These effects induce the damping of the coherence for upper polariton states and lead to the invisible dispersion of the UPB.
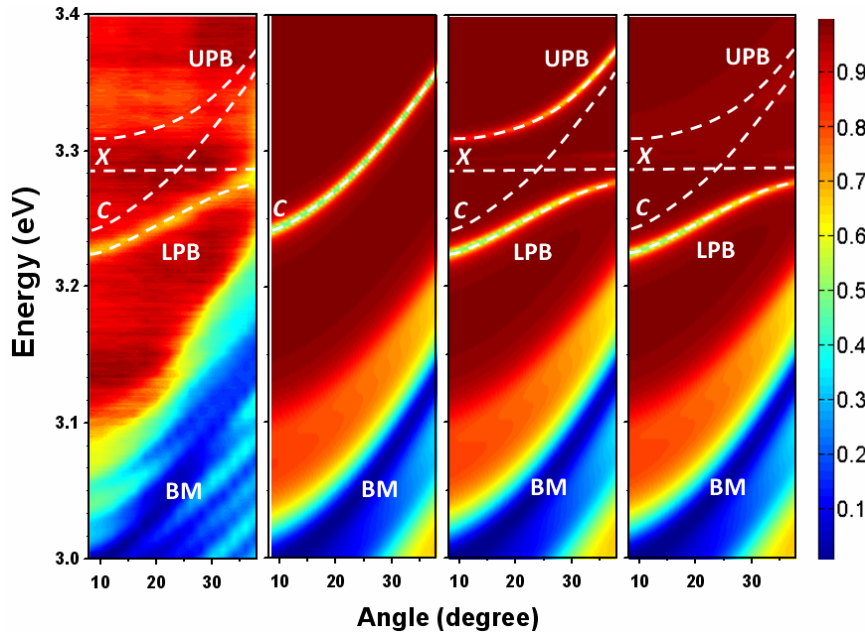

Fig. 31. (a) Color map of the angular dispersion of measured reflectivity spectra from 8 to 38° at RT. (b) Color maps of the calculated angle-resolved reflectivity spectra without taking the resonant exciton into account. (c) Color maps of the calculated angle-resolved reflectivity spectra with taking the resonant exciton into account. (d) Simulation of angle-resolved reflectivity spectra for the bulk ZnO MCs after taking the absorption continuum into account.

To further confirm our experimental results and get further insight into the significant influence of the continuum states, we prepared a ZnO MC with relatively thinner cavity thickness, i.e., smaller exciton-cavity detuning. Fig. 31 (a) shows the color map of the measured angle-resolved reflectivity spectra of the ZnO MC with smaller detuning. Similar situations

including non-parabolic LPB and invisible UPB are observed in Fig. 31(a). The simulation of angle-resolved reflectivity spectra for the pure cavity mode and the polariton modes are shown in Figs. 31(a) and 31(b), respectively. Based on identical simulation parameters, the calculated LPB is also in good agreement with the measured results. An identical vacuum Rabi splitting value is obtained at the resonant angle of about 24°. Moreover, the calculated angle-resolved reflectivity spectra including the continuum absorption is plotted in Fig. 31(d), which is also in good agreement with measured results. By comparing Figs. 30(a) and 31(a), the different exciton-polariton dispersion curves due to different detuning values can be obviously observed. Consequently, the evidence for exciton-photon strong coupling in bulk ZnO MCs at RT is confirmed by the observation of the lower polariton dispersion curves from two different detuning values. Although the full anticrossing behavior cannot be experimentally demonstrated because of the strong continuum absorption, it should be noted that clear observation of the LPB is more important for the investigation of Bose-Einstein condensation and polariton lasing. Prospects regarding the experimental observation of the complete anticrossing behavior may be achieved based on a ZnO/ZnMgO QW-MC due to the decrease in the thickness of ZnO absorption and the enhancement of exciton binding energies, pushing the continuum states of exciton to higher energy values.

(五) 參考文獻

[1] K. Iga, "Surface-emitting laser-its birth and generation of new optoelectronics field," IEEE J. Select. Topics Quantum Electron., vol. 6, no. 6, pp. 1201–1215, Nov. 2000.

[2] W. W. Chow, K. D. Choquette, M. H. Crawford, K. L. Lear, and G. R. Hadley, "Design, fabrication, and performance of infrared and visible vertical-cavity surface-emitting lasers," IEEE J. Quantum Electron., vol. 33, no. 10, pp. 1810–1824, Oct. 1997.

[3] E. Towe, R. F. Leheny, and A. Yang, "A historical perspective of the development of the vertical-cavity surface-emitting laser," IEEE J. Select. Topics Quantum Electron., vol. 6, no. 6, pp. 1458–1464, Nov./Dec. 2000.

[4] H. Soda, K. Iga, C. Kitahara, Y. Suematsu, GaInAsP/InP surface emitting injection lasers, Jpn. J. Appl. Phys. **18**(12), 2329 (1979)

[5] G. S. Huang, T. C. Lu, H. H. Yao, H. C. Kuo, S. C. Wang, C.-W. Lin, and L. Chang, "Crack-free GaN/AlN distributed Bragg reflectors incorporated with GaN/AlN superlattices grown by metalorganic chemical vapor deposition," Appl. Phys. Lett., vol. 88, pp. 061904, 2006.

[6] E. Yablonovitch, "Inhibited spontaneous emission in solid-state physics and electronics," Phys. Rev. Lett., vol. 58, pp. 2059–2062, Dec. 1987.

[7] S. John, "Strong localization of photons in certain disordered dielectric superlattices," Phys. Rev. Lett., vol. 58, pp. 2486–2489, Mar. 1987.

[8] J. D. Joannopoulos, P. R. Villeneuve, and S. Fan, "Photonic crystals: Putting a new twist on light," Nature, vol. 386, pp. 143–149, Mar. 1997.

[9] O. Painter, R. K. Lee, A. Scherer, A. Yariv, J. D. O'Brien, P. D. Dapkus, and I. Kim,

"Two-dimensional photonic band-gap defect mode laser,"Science, vol. 284, pp. 1819–1821, Jun. 1999.

[10] H. G. Park, S. H. Kim, S. H. Kwon, Y. G. Ju, J. K. Yang, J. H. Baek, S. B. Kim, and Y. H. Lee, "Electrically driven single-cell photonic crystal laser," Science, vol. 305, pp. 1444–1447, Sep. 2005.

[11] M. Meier, A. Mekis, A. Dodabalapur, A. Timko, R. E. Slusher, J. D. Joannopoulos, and O. Nalamasu, Appl. Phys. Lett. 74, 7 (1999)

[12] M. Imada, S. Node, A. Chutinan, and T. Tokuda, Appl. Phys. Lett. 75, 316 (1999)

[13] D. Ohnishi, T. Okano, M. Imada, and S. Node, Opt. Express 12, 1562 2004.

[14] S. Ogawa, M. Imada, S. Yoshimoto, M. Okano, and S. Noda, Science 305, 227 2004.

[15] C. Weisbuch, M. Nishioka, A. Ishikawa, and Y. Arakawa1, Phys. Rev. Lett. **69**, 3314 (1992).

[16] G. Christmann, R. Butté, E. Feltin, J.-F. Carlin, and N. Grandjean, Appl. Phys. Lett. **93**, 051102 (2008).

[17] S. I. Tsintzos, N. T. Pelekanos, G. Konstantinidis, Z. Hatzopoulos, and P. G. Savvidis, Nature **453**, 372 (2008).

[18] M. Saba, C. Ciuti, J. Bloch, V. Thierry-Mieg, R. André, L. S. Dang, S. Kundermann, A. Mura, G. Bongiovanni, J. L. Staehli, and B. Beveaud, Nature **414**, 731 (2001).

[19] S. I. Tsintzos, P. G. Savvidis, G. Deligeorgis, Z. Hatzopoulos, and N. T. Pelekanos, Appl. Phys. Lett. **94**, 071109 (2009).

[20] K. Kornitzer, T. Ebner, K. Thonke, R. Sauer, C. Kirchner, V. Schwegler, M. Kamp, M. Leszczynski, I. Grzegory, and S. Porowski, Phys. Rev. B **60**, 1471 (1999).

[21] G. Christmann, R. Butté, E. Feltin, A. Mouti, P. A. Stadelmann, A. Castiglia, J.-F. Carlin, and N. Grandjean, Phys. Rev. B **77**, 085310 (2008).

[22] J. M. Redwing, D. A. S. Loeber, N. G. Anderson, M. A. Tischler, and J. S. Flynn, "An optically pumped GaN-AlGaN vertical cavity surface emitting laser," Appl. Phys. Lett., vol. 69, pp. 1–3, 1996.

[23] T. Someya, K. Tachibana, J. Lee, T. Kamiya, and Y. Arakawa, "Lasing emission from an $In_{0.1}Ga_{0.9}N$ vertical cavity surface emitting laser," Jpn. J. Appl. Phys., vol. 37, pp. L1424–L1426, 1998.

[24] Y.-K. Song, H. Zhou, M. Diagne, I. Ozden, A. Vertikov, A. V. Nurmikko, C. Carter-Coman, R. S. Kern, F. A. Kish, and M. R. Krames, "A vertical cavity light emitting InGaN quatnum well heterostructure," Appl. Phys. Lett., vol. 74, pp. 3441–3443, 1999.

[25] T. Someya, R. Werner, A. Forchel, M. Catalano, R. Cingolani, and Y. Arakawa, "Room temperature lasing at blue wavelengths in gallium nitride microcavities," Science, vol. 285, pp. 1905–1906, 1999.

[26] J.-F. Carlin, J. Dorsaz, E. Feltin, R. Butté, N. Grandjean, M. Ilegems, and M. Laügt, "Crack-free fully epitaxial nitride microcavity using highly reflective AlInN/GaN Bragg mirrors," Appl. Phys. Lett., vol. 86, pp. 031107, 2005.

[27] H. Zhou, M. Diagne, E. Makarona, A. V. Nurmikko, J. Han, K. E. Waldrip, J. J. Figiel, Near ultraviolet optically pumped vertical cavity laser, Electron. Lett. **36**, 1777 (2000)

[28] S.-H. Park, J. Kim, H. Jeon, T. Sakong, S.-N. Lee, S. Chae, Y. Park, C.-H. Jeong, G.-Y. Yeom,

Y.-H. Cho, Room-temperature GaN vertical-cavity surface-emitting laser operation in an extended cavity scheme, Appl. Phys. Lett. **83**, 2121 (2003)

[29] T. Tawara, H. Gotoh, T. Akasaka, N. Kobayashi, T. Saitoh, Low-threshold lasing of InGaN vertical-cavity surface-emitting lasers with dielectric distributed Bragg reflectors, Appl. Phys. Lett. **83**, 830 (2003)

[30] E. Feltin, G. Christmann, J. Dorsaz, A. Castiglia, J.-F. Carlin, R. Butté, N. Grandjean, S. Christopoulos, G. Baldassarri, H. von Högersthal, A. J. D. Grundy, P. G. Lagoudakis, J. J. Baumberg, Blue lasing at room temperature in an optically pumped lattice-matched AlInN/GaN VCSEL structure, Electron. Lett. **43**, 924 (2007)

[31] J.-T. Chu, T.-C. Lu, H.-H. Yao, C.-C. Kao, W.-D. Liang, J.-Y. Tsai, H.-C. Kuo, S.-C. Wang, Room-temperature operation of optically pumped blue-violet GaN-based vertical-cavity surface-emitting lasers fabricated by laser lift-off, Jpn. J. Appl. Phys. **45**, 2556 (2006)

[32] J.-T. Chu, T.-C. Lu, M. You, B.-J. Su, C.-C. Kao, H.-C. Kuo, S.-C. Wang, Emission characteristics of optically pumped GaN-based vertical-cavity surface-emitting lasers, Appl. Phys. Lett. **89**, 121112 (2006)

[33] C.-C. Kao, Y. C. Peng, H. H. Yao, J. Y. Tsai, Y. H. Chang, J. T. Chu, H. W. Huang, T. T. Kao, T. C. Lu, H. C. Kuo, S. C. Wang, Fabrication and performance of blue GaN-based vertical-cavity surface emitting laser employing AlN/GaN and Ta_2O_5/SiO_2 distributed Bragg reflector, Appl. Phys. Lett. **87**, 081105 (2005)

[34] C.-C. Kao, T. C. Lu, H. W. Huang, J. T. Chu, Y. C. Peng, H. H. Yao, J. Y. Tsai, T. T. Kao, H. C. Kuo, S. C. Wang, C. F. Lin, The lasing characteristics of GaN-based vertical-cavity surface-emitting laser with AlN-GaN and Ta_2O_5-SiO_2 distributed Bragg reflectors, IEEE Photon. Technol. Lett. **18**, 877 (2006)

[35] T-C. Lu, C.-C. Kuo, H.-C. Kuo, G.-S. Huang, S.-C. Wang, CW lasing of current injection blue GaN-based vertical cavity surface emitting laser, Appl. Phys. Lett. **92**, 141102 (2008)

[36] Y. Higuchi, K. Omae, H. Matsumura, T. Mukai, Room-temperature CW lasing of a GaN-based vertical-cavity surface-emitting laser by current injection, Appl. Phys. Express **1**, 121102 (2008)

[37] S. H. Kwon, H. Y. Ryu, G. H. Kim, Y. H. Lee, and S. B. Kim, "Photonic bandedge lasers in two-dimensional square-lattice photonic crystal slabs,"Appl. Phys. Lett., vol. 83, pp. 3870–3872, Nov. 2003.

[38] M. Notomi, H. Suzuki, and T. Tamamura, "Directional lasing oscillation of two-dimensional organic photonic crystal lasers at several photonic band gaps," Appl. Phys. Lett., vol. 78, pp. 1325–1327, Mar. 2001.

[39] H.Matsubara, S. Yoshimoto, H. Saito, Y. Jianglin, Y. Tanaka, and S. Noda,"GaN photonic-crystal surface-emitting laser at blue-violet wavelengths,"Science, vol. 319, pp. 445–447, Jan. 2008.

[40] N. Antoine-Vincent, F. Natali, F. Byrne, A. Vasson, P. Disseix, J. Leymarie, M. Leroux, F. Semond, and J. Massies, "Observation of Rabi splitting in a bulk GaN microcavity grown on silicon", Phys. Rev. B, vol.68, pp. 153313/1-4, Oct. 2003.

[41] S. Christopoulos, G. Baldassarri Höger von Högersthal, A. J. D. Grundy, P. G. Lagoudakis, A.

V. Kavokin, J. J. Baumberg, G. Christmann, R. Butté, E. Feltin, J. –F. Carlin, and N. Grandjean, "Room temperature polariton lasing in semiconductor microcavities", Phys. Rev. Lett., vol. 98, pp. 126405/1-4, Mar. 2007.

[42] M. Zamfirescu, A. Kavokin, B. Gil, G. Malpuech, and M. Kaliteevski, Phys. Rev. B **65**, 161205 (2002).

[43] R. Johne, D. D. Solnyshkov, and G. Malpuech, Appl. Phys. Lett. **93**, 211105 (2008).

[44] F. Médard, J. Zúñiga-Perez, P. Disseix, M. Mihailovic, J. Leymarie, A. Vasson, F. Semond, E. Frayssinet, J. C. Moreno, M. Leroux, S. Faure, and T. Guillet, Phys. Rev. B **79**, 125302 (2009).

[45] R. Shimada, J. Xie, V. Avrutin, Ü. Özgür, and H. Morkoč, Appl. Phys. Lett. **92**, 011127 (2008).

[46] J.-R. Chen, T.-C. Lu, Y.-C. Wu, S.-C. Lin, W.-R. Liu, W.-F. Hsieh, C.-C. Kuo, and C.-C. Lee, Appl. Phys. Lett. **94**, 061103 (2009).

[47] S. Faure, T. Guillet, P. Lefebvre, T. Bretagnon, and B. Gil, Phys. Rev. B **78**, 235323 (2008).

[48] F. A. Ponce, D. P. Bour, Nitride-based semiconductors for blue and green light-emitting devices, Nature, **386**, 351 (1997)

[49] J.-F. Carlin, M. Ilegems, High-quality AlInN for high index contrast Bragg mirrors lattice matched to GaN, Appl. Phys. Lett. **83**, 668 (2003)

[50] K. Iga, Possibility of Green/Blue/UV surface emitting lasers, in Int. Symp. Blue Laser and Light Emitting Diodes, No. Th-11, 263 (Mar. 1996)

[51] J.-T. Chu, T.-C. Lu, H.-H. Yao, C.-C. Kao, W.-D. Liang, J.-Y. Tsai, H.-C. Kuo, S.-C. Wang, Room-temperature operation of optically pumped blue-violet GaN-based vertical-cavity surface-emitting lasers fabricated by laser lift-off, Jpn. J. Appl. Phys. **45**, 2556 (2006)

[52] S. Kako, T. Someya, Y. Arakawa, Observation of enhanced spontaneous emission coupling factor in nitride-based vertical-cavity surface-emitting laser, Appl. Phys. Lett. **80**, 722 (2002)

[53] W. S. Wong, T. Sands, N. W. Cheung, M. Kneissl, D. P. Bour, P. Mei, L. T. Romano, N. M. Johnson, Fabrication of thin-film InGaN light-emitting diode membranes by laser lift-off, Appl. Phys. Lett. **75**, 1360 (1999)

[54] S.-H. Park, Crystal orientation effects on many-body optical gain of wurtzite InGaN/GaN quantum well lasers, Jpn. J. Appl. Phys. **42**, L170 (2003)

[55] A. Kaneta, K. Okamoto, Y. Kawakami, S. Fujita, G. Marutsuki, Y. Narukawa, T. Mukai, Spatial and temporal luminescence dynamics in an $In_xGa_{1-x}N$ single quantum well probed by near-field optical microscopy, Appl. Phys. Lett. **81**, 4353 (2002)

[56] B. Witzigmann, V. Laino, M. Luisier, U. T. Schwarz, G. Feicht, W. Wegscheider, K. Engl, M. Furitsch, A. Leber, A. Lee, V. Härle, Microscopic analysis of optical gain in InGaN/GaN quantum wells, Appl. Phys. Lett. **88**, 021104 (2006)

[57] Plihal and A. A. Maradudin, "Photonic band structure of two-dimensional systems: The triangular lattice", Phys. Rev. B, vol 44, pp 8565-856 ,Feb 1991.

[58] K. Sakai, J. Yue, S. Noda, "Coupled-wave model for triangular-lattice photonic crystal with transverse electric polarization '',Optics Express , vol 16, No.9, pp 6033-6040 ,Apr. 2008.

[59] M. Imada, A. Chutinan, S. Noda, M. Mochizuki, ''Multidirectionally distributed feedback

photonic crystal lasers'', Phys. Rev. B, vol 65 ,pp 195306, Apr. 2002.

[60] M. Notomi, H. Suzuki, and T. Tamamura, ''Directional lasing oscillation of two-dimensional organic photonic crystal lasers at several photonic band gaps'', Appl. Phys. Lett., vol 78, pp 1325-1327, March 2001.

[61] A. Tsukazaki, A. Ohtomo, T. Onuma, M. Ohtani, T. Makino, M. Sumiya, K. Ohtani, S. F. Chichibu, S. Fuke, Y. Segawa, H. Ohno, H. Koinuma, and M. Kawasaki, Nat. Mater. **4**, 42 (2005).

[62] Z. K. Tang, G. K. L. Wong, P. Zu, M. Kawasaki, A. Ohtomo, H. Koinuma, and Y. Segawa, Appl. Phys. Lett. **72**, 3270 (1998).

[63] K. Vanheusden, C. H. Seager, W. L. Warren, D. R. Tallant, and J. A. Voigt, Appl. Phys. Lett. **68**, 403 (1996).

[64] Y. Chen, D. M. Bagnall, H. Koh, K. Park, K. Hiraga, Z. Zhu, and T. Yao, J. Appl. Phys. **84**, 3912 (1998).

[65] E. S. Shim, H. S. Kang, J. S. Kang, J. H. Kim, and S. Y. Lee, Appl. Surf. Sci. **186**, 474 (2002).

[66] N. Antoine-Vincent, F. Natali, D. Byrne, A. Vasson, P. Disseix, J. Leymarie, M. Leroux, F. Semond, and J. Massies, Phys. Rev. B **68**, 153313 (2003).

[67] W. Y. Liang and A. D. Yoffe, Phys. Rev. Lett. **20**, 59 (1968)

(六) 與國外學術合作

In this project, we have collaborated with Prof. Iga and Prof. Koyama of Tokyo Institute of Technology to conduct the research of CW electrically pumped GaN VCSELs. Prof. Iga is the inventor of VCSELs and a world class expert in the research of VCSELs. The experience gained from Prof. Iga and Prof. Koyama on the GaAs-based VCSELs is very useful for this effort and ensures the successful outcome of this experiment. We also collaborated with Prof. Yamamoto and Prof. Fan of Stanford University to establish the theoretical analysis of GaN microcavity and GaN PCSELs. Besides, we also collaborate with many international experts in different fields.

Affiliation	Professor	Topic
Tokyo Institute of Technology	Prof. Iga	GaN VCSELs
Tokyo Institute of Technology	Prof. Koyama	GaN VCSELs
Stanford University	Prof. Yamamoto	GaN microcavity
Stanford University	Prof. Fan	GaN PCSELs
University of Illinois at Urbana Champaign	Prof. S. L. Chuang	Design of QWs
Yale University	Prof. Han	Epitaxy of GaN materials
Rensselaer Polytechnic Institute	Prof. S.-Y. Lin	Photonic crystal design
Kyoto University	Prof. Noda	GaN PCSELs

(七) 計畫成果自評

The main objective of this proposed research project is to investigate the basic properties of mesoscopic GaN-based quantum confined structures by means of nano fabrication techniques related to the material, electrical and optical aspects and of the novel methodology to achieve controlled photon emission from the GaN-based quantum confined structures. The specific objectives of this proposal include:

(1) Establishment of the fabrication technology of GaN quantum confined structures such as quantum dots and nanostructures;

(2) Simulation and modeling of the optical properties of a high-Q microcavity and development of device design guidelines for fabrication of microcavity quantum confined structures;

(3) Fabrication of devices incorporating the quantum confined structures into a high-Q microcavity;

(4) Investigation of the optical properties of the fabricated quantum confined structures and microcavity structures;

(5) Investigation and demonstration of the controlled photon emission from the microcavity

quantum confined structures or devices.

This project has the following major impacts and contributions to the domestic academic potential and capability as well as the international academic status of our country. These are briefly described below.

1. Our research project is focused on the high efficiency nitride-based light emitting devices. We have demonstrated the first electrically pumped GaN VCSEL at 77 K in the world. The lasing action of GaN PCSELs was also observed under optical pumping at RT. These two kinds of blue vertical-cavity semiconductor lasers are important light sources for the applications of laser projector, laser display, and high-density optical storage system. As for the study of GaN-based microcavity exciton polaritons, they are one kind of the important single photon light sources and critical approaches to achieve RT Bose-Einstein condensation in solid. The microcavity polaritons are also an approach to fabricate thresholdless polariton lasers. Furthermore, GaN-based blue and ultraviolet LEDs are promising light sources for the future solid-state lighting. Thus the program will not only enhance the academic research capability of our team members in particular but also our country in general. The outcomes of this research project could also contribute to the national development and related applications of nanotechnology.

2. This program will train many research team members including graduate students, postdoctors, and technical staff with multiple disciplinary knowledge and skills. These members will become the main workforce for the emerging nanotechnology related industry and new information technology of our country.

3. Our research subject is a frontier research topic currently being pursued by the leading international research teams in USA, Japan, France, and Germany. Our research effort on this subject will promote the international academic status and visibility of our country.

4. The development of high efficiency nitride-based light emitting devices, including GaN VCSELs, PCSELs, nanolasers, and LEDs is critical for the academic research and industry development. They will provide a key enabling component for the emerging new applications and make a major contribution to this new and revolutional information technology of the new aera.

發表之期刊論文列表

Journal paper
2006

[1] Te-Chung Wang, Tien-Chang Lu, Tsung-Shine Ko, Hou-Guang Chen, Hao-Chung Kuo, Min Yu,Chang-Cheng Chuo, and Zheng-Hong Lee, "Trenched Epitaxial Lateral Overgrowth of Fast Coalesced *a*-plane GaN with Low Dislocation Density", Appl. Phys. Lett., V89, 251109, (Dec, 19, 2006)

[2] Hung-Wen Huang, C. F. Lai, W. C. Wang, T. C. Lu, H. C. Kuo, and S. C. Wang, "Efficiency Enhancement of GaN-based Power Chip LEDs With Sidewall Roughness By Natural Lithography", Electrochem. Solid State Lett., V10 (2): H59-H62, (Dec. 14, 2006)

[3] Tsan-Wen Lu, Po-Tsung Lee, Feng-Mao Tsai, and Tien-Chang Lu, "Investigation of Whispering Gallery Mode Dependence on Cavity Geometry of Quasi-Periodic Photonic Crystal Micro-Cavity Lasers", Appl. Phys. Lett., V89, 231111, (Dec. 6, 2006)

[4] Hung-Lu Chang, T. C. Lu, H. C. Kuo, and S. C. Wang, "Effect of oxygen on nickel oxide / indium tin oxide heterojunction diodes at room temperature", V100, 124503, J. Appl. Phys., (Dec. 15, 2006)

[5] Y. J. Lee, H.C. Kuo, T.C. Lu, and S. C. Wang, "High Light-Extraction GaN-based Vertical LEDs With Double Diffuse Surfaces", IEEE J. Quantum. Electron. V42, No.12, pp.1196-1201, (Dec., 2006)

[6] C.H. Lin, C.F. Lai, T. S. Ko, H. W. Huang, H. C. Kuo, Y. Y. Hung, K. M. Leung, C. C. Yu, R. J. Tsai, C. K. Lee, T. C. Lu, and S. C. Wang, "Enhancement of InGaN–GaN Indium–Tin–Oxide Flip-Chip Light-Emitting Diodes With TiO$_2$–SiO$_2$ Multilayer Stack Omnidirectional Reflector", V18, Issue 19, pp2050-2052, IEEE Photon. Tech. Lett (Oct.1, 2006)

[7] Y. J. Lee, H.C. Kuo, T.C. Lu, B. J. Su, and S. C. Wang, "Fabrication and characterization of GaN-based LEDs grown on chemical wet-etched patterned sapphire substrates", V153, I12, ppG1106-G1111 J. Electrochem. Soc., (23 Oct, 2006)

[8] T. S. Ko, H. C. Hsu, S. Yang, C. P. Chu, H. F. Lin, S. C. Liao, T. C. Lu, H. C. Kuo, W. F. Hsieh, and S. C. Wang, "Optical properties of ZnO nanopowders fabricated by DC thermal plasma synthesis", V134, Issue1, pp54-58, Materials Science and Engineering: B, (25 Sept., 2006)

[9] Jung-Tang Chu, Tien-chang Lu, Hsin-Hung Yao, Chih-Chiang Kao, Wen-Deng. Liang, Jui-Yen Tsai, Hao-chung Kuo and Shing-Chung Wang, "Emission Characteristics of Optically Pumped GaN-based Vertical-Cavity Surface-Emitting Lasers", Appl. Phys. Lett., V89, pp121112, (18 Sept, 2006)

[10] Yi-An Chang, Tsung-Hsine Ko, Fang-I Lai, Jun-Rong Chen, Chun-Lung Yu, I-Tsung Wu, Hao-Chung Kuo, Yen-Kuang Kuo, Li-Wen Laih, Li-Horng Laih, Tien-Chang Lu, and Shing-Chung

Wang, "Carrier blocking effect on 850-nm InAlGaAs/AlGaAs vertical-cavity surface-emitting lasers",V21, pp1488-1494, Semicon. Sci. Tech, (Sept. 11, 2006)

[11] Yi-An Chang, Chun-Lung Yu, I-Tsung Wu, Hao-Chung Kuo, Fang-I Lai, Li-Wen Laih, Li-Horng Laih, Tien-Chang Lu, and Shing-Chung Wang, "Design and Fabrication of Temperature Insensitive InGaP/InGaAlP Resonant-Cavity Light-Emitting Diodes", V18, No.16, pp1690-1692, IEEE Photon. Tech. Lett, (August, 2006)

[12] T. S. Ko, C. P. Chu, H. G. Chen, T. C. Lu, H. C. Kuo, and S. C. Wang, "Observation of Strong Red Photoluminescence with Broad Band in Indium Oxy-nitride Nanoparticles", J. Vac. Sci. Technol. A, V24, No.4, (Jul/Aug, 2006) and was selected Virtual Journal of Nanoscale Science & Technology -- July 4, 2006

[13] Hung-Wen Huang, H. C. Kuo, J. T. Chu, C. F. Lai, C.C. Kao, T. C. Lu, S. C.Wang, R. J. Tsai, C. C. Yu, and C. F. Lin, "Nitride-Based LEDsWith Nano-scale Textured Sidewalls Using Natural Lithography", NanoTechnology, V17, No12, pp2998-3001, (Jun 28 2006)

[14] G.S. Huang, H. H. Yao, T. C. Lu, H.C. Kuo, and S. C. Wang, "Aluminum incorporation into AlGaN grown by low-pressure metalorganic vapor phase epitaxy", J. Appl. Phys., V99, 104901, (24 May, 2006)

[15] Po-Tsung Lee, Tsan-Wen Lu, Feng-Mao Tsai, Tien-Chang Lu, and Hao-Chung Ku, "Whispering gallery mode of modified octagonal quasiperiodic photonic crystal single-defect microcavity and its side-mode reduction", Appl. Phys. Lett., V88, 201104, (May, 2006)

[16] Y. J. Lee, J.M.Hwang, T. C. Hsu, M. H. Hsieh, M. J. Jou, B. J. Lee, T.C. Lu, H.C. Kuo, and S.C. Wang, "Enhancing the Output Power of GaN-based LEDs Grown on Chemical Wet Etching Patterned Sapphire Substrate", IEEE Photon. Tech. Lett., V18, No.10, pp1152-1155, (May, 2006)

[17] Te-Chung Wang, Hao-Chung Kuo, Tien-Chang Lu, Ching-En Tsai, Min-Ying Tsai, Jung-Tsung Hsu, Jer-Ren Yang, "Study of InGaN multiple Quantum Dots by MOCVD", Jpn. J. Appl. Phys., Vol. 45, No. 4B, pp. 3560-3563 (April, 25, 2006)

[18] Y. C. Peng, C. C. Kao, H. W. Huang, J. T. Chu, T. C. Lu, H. C. Kuo, and S. C. Wang, "Fabrication and characteristics of GaN-based microcavity LEDs with high reflectivity AlN/GaN DBRs", Jpn. J. Appl. Phys., Vol. 45, No. 4B, pp. 3446-3448 (April, 25, 2006)

[19] Hung-Wen Huang, Jung-Tang Chu, Chih-Chiang Kao, Tao-Hung Hsueh, Tien-Chang Lu, Hao-Chung Kuo, and Shing-Chung Wang, "Enhanced Light Output in InGaN/GaN Light Emitting Diodes with Excimer Laser Etching surfaces", Jpn. J. Appl. Phys., Vol. 45, No. 4B, pp. 3442-3445, (April, 25, 2006)

[20] J.T. Chu, T.C. Lu, H.H. Yao, C.C. Kao, W.D. Liang, J.Y. Tsai, H.C. Kuo and S.C. Wang, "Laser lift-off fabrication of blue-violet GaN-based vertical cavity surface emitting lasers optically pumped at room temperature", Jpn. J. Appl. Phys., V45, No.4A, pp2556-2560, (April, 2006)

[21] Chih-Chiang Kao, T. C. Lu, H. W. Huang, J. T. Chu, Y. C. Peng, H. H. Yao, J. Y. Tsai, T. T. Kao, H. C. Kuo, S. C. Wang and C. F. Lin "A high characteristic temperature GaN-based vertical-cavity surface emitting laser", IEEE Photon. Tech. Lett, V18, No.7, pp877-879, (April, 2006)

[22] Y. J. Lee, J.M.Hwang, T. C. Hsu, M. H. Hsieh, M. J. Jou, B. J. Lee, T.C. Lu, H.C. Kuo, and S.C. Wang, "GaN-based LEDs with Al-Deposited V-Shape Sapphire Facet Mirror", IEEE Photon. Tech. Lett, V18, No.5, pp724-726, (March, 2006)

[23] Yi-An Chang, Sheng-Horng Yen, Te-Chung Wang, Hao-Chung Kuo ,Yen-Kuang Kuo, Tien-Chang Lu, and Shing-Chung Wang "Experimental and Theoretical Analysis on Ultraviolet 370-nm AlGaInN Light-Emitting Diodes", Semicon. Sci. Tech., V21, pp598-603 (21 March, 2006)

[24] H. H. Yao, T. C. Lu, G. S. Huang, C. Y. Chen, W. D. Liang, H. C. Kuo and S. C. Wang, "InGaN self-assembled quantum dots grown by metalorganic chemical-vapor deposition with interruption growth", NanoTechnology, V17, pp1713-1716, (27 Feb 2006)

[25] G.S. Huang, T. C. Lu, H. H. Yao, H.C. Kuo, S. C. Wang, Chih-wei Lin and Li Chang "Crack-free GaN/AlN distributed Bragg reflectors incorporated with GaN/AlN superlattices grown by metal-organic chemical vapor deposition", Appl. Phys. Lett., V88, 061904, (Feb, 2006)

[26] Y. J. Lee, T.C. Lu, H.C. Kuo, S.C. Wang, M. J. Liou, C.W. Chang, T. C. Hsu, M. H. Hsieh, M. J. Jou, and B. J. Lee, "High Brightness AlGaInP-based Light Emitting Diodes with the Stripe Patterned Omni-Directional Reflector", Semicon. Sci. Tech., V11, pp1-6, (Feb, 2006)

[27] Y. J. Lee, T.C. Lu, H.C. Kuo, S.C. Wang, M. J. Liou, C.W. Chang, T. C. Hsu, M. H. Hsieh, M. J. Jou, and B. J. Lee, "AlGaInP LEDs with Stripe Patterned Omni-Directional Reflector", Jpn. J. Appl. Phys., V45(2A), pp643-645, (Feb, 2006)

[28] Te-Chung Wang, Hao-Chung Kuo, Zheng-Hong Lee, Chang-Cheng Chuo, Min-Ying Tsai, Ching-En Tsai, Tsin-Dong Lee, Tien-Chang Lu, Jim Chi, "Quaternary AlInGaN multiple quantum well 368nm light-emitting diode", J. Crystal Growth, V287 pp582-585, (Jan, 2006)

2007

[1] M. D. Yang, J. L. Shen, M. C. Chen, C. C. Chiang, S. M. Lan , T. N. Yang , M. H. Lo, H. C. Kuo , Tien-Chang Lu , "Optical studies of InN epilayers on Si substrates with different buffer layers", J. Appl. Phys., V102, 113514, (Dec. 8, 2007)

[2] C. H. Chiu, T. C. Lu, H. W. Huang, C. F. Lai, C. C. Kao, J. T. Chu, C. C. Yu, H. C. Kuo, and S. C. Wang, C. F. Lin, T. H. Shueh, "Fabrication of InGaN/GaN MQW nanorods LED by ICP-RIE and PEC oxidation process with self-assembly Ni metal islands", Nanotechnology, V18, N.44, p445201 (Nov. 7, 2007)

[3] Tien-Chang Lu, Tsung-Ting Kao, Chih-Chiang Kao, Jung-Tang Chu, Kang-Fan Yeh, Li-Fan Lin, Yu-Chun Peng, Hung-Wen Huang, Hao-Chung Kuo, and Shing-Chung Wang

"GaN-Based High-Q Vertical-cavity Light Emitting Diodes", IEEE Electron. Device Lett., V28, N10, pp884, (Oct., 2007)

[4] C. H. Chiu, H. C. Kuo, C. F. Lai, H. W. Huang, W. C. Wang, T. C. Lu, S. C. Wang, and C. H. Lin, "Enhancement of InGaN/GaN Flip-Chip ITO LEDs with Incline Sidewalls Coated with TiO2/SiO2 Omnidirectional Reflector", J. Electrochem. Soc., V154, Issue 11, pp. H944-H947 (Sept. 6, 2007)

[5] Shing-Chung Wang, Tien-Chang Lu, Chih-Chiang Kao, Jong-Tang Chu, Gen-Sheng Huang, Hao-Chung Kuo, Shih-Wei Chen, Tsung-Ting Kao, Jun-Rong Chen, and Li-Fan Lin, "Optically Pumped GaN-based Vertical Cavity Surface Emitting Lasers: Technology and Characteristics", Jpn. J. Appl. Phys., V46, No. 8B, pp5397-5407, (Aug. 23, 2007)

[6] C. H. Chiu, M. H. Lo, C. F. Lai, T. C. Lu, Y. A. Chang, H. W. Huang, H. C. Kuo, S. C. Wang, C. F. Lin, and Y. K. Kuo, "Optical properties of high Indium $In_{0.3}Ga_{0.7}N$/GaN MQW green nanorods by plasma etching with nanoscale nickel metal islands", Nanotechnology, V18, N33, p335706, (Aug. 23, 2007)

[7] C. E. Lee, Y. J. Lee, H. C. Kuo, M. R. Tsai, B. S. Cheng, T. C. Lu, S. C. Wang, C. T. Kuo, "Enhancement of Flip-Chip Light-Emitting Diodes With Omni-Directional Reflector and Textured Micropillar Arrays", IEEE Photon. Tech. Lett., V19, No16, pp1200-1202, (Aug. 15, 2007)

[8] Chun-Feng Lai, Peichen Yu, Te-Chung Wang, Hao-Chung Kuo, Tien-Chang Lu, Shing-Chung Wang and Chao-Kuei Lee "Lasing Characteristics of a GaN Photonic Crystal Nanocavity Light Source", Appl. Phys. Lett., V91, 041101, (Jul. 23, 2007) and was selected in Virtual Journal of Nanoscale Science & Technology – Aug. 6, 2007 V16, Issue 6

[9] T. S. Ko, C. P. Chu, T. C. Lu, H. C. Kuo, and S. C. Wang "Synthesis of In_2O_3 nanocrystal chains and annealing effect on their optical properties", J. Vac. Sci. Technol. A, V25, pp1038-1041 (Jul 2, 2007) and was selected in Virtual Journal of Nanoscale Science & Technology -- July 16, 2007

[10] Y.C. Lee, H.C. Kuo, C.E. Lee, J.R. Chen, Y.A. Chang, T.C. Lu, S.C. Wang, and S.W. Chiou, "High Temperature Stability of 650-nm Resonant-Cavity Light-Emitting Diodes Fabricated Using Wafer Bonding Technique on Silicon Substrates", IEEE Photon. Tech. Lett., V19, No14, pp1060-1062, (Jul 15, 2007)

[11] Hou-Guang Chen, T. S. Ko, Tien-Chang Lu, Hao-Chung Kuo and Shing-Chung Wang, Li Chang, "Dislocation reduction in non-polar GaN grown on stripe patterned r-plane sapphire substrates", Appl. Phys. Lett., V91, 021914, (Jul. 9, 2007)

[12] G. S. Huang, T. C. Lu, H. C. Kuo and S. C. Wang and Hou-Guang Chen, "Fabrication of hybrid nitride microcavity with high quality factor using highly reflective AlN/GaN and

Ta$_2$O$_5$/SiO$_2$ distributed Bragg mirrors", IEEE Photon. Tech. Lett., V19, No13, pp999-pp1001, (July 1, 2007)

[13] G. S. Huang, H. C. Kuo, M. H. Lo, T. C. Lu, S. C. Wang, and J. Y. Tsai, "Improvement of efficiency and ESD characteristics of ultraviolet light emitting diodes by inserting AlGaN and SiN buffer layers", J. Crystal Growth, V305, pp55-58, (July 1, 2007)

[14] C. H. Chiu, H.C. Kuo, C. E. Lee, C. H. Lin, P.C. Cheng, H. W. Huang, T.C. Lu, S. C. Wang, and K. M. Leung, "Fabrication and Characteristics of thin-film InGaN–GaN light-emitting diodes with an TiO$_2$/SiO$_2$ omnidirectional reflector", Semicon. Sci. Tech, V22, p831-835, (Jun. 21, 2007)

[15] Chih-Chiang Kao, Kang-Fan Yeh, Jong-Tung Chu, Wei-Lun Peng, Hung-Wen Huang, Tien-Chang Lu, Hao-Chung Kuo and Shing-Chung Wang, "Light-Output Enhancement of Nano-Roughened GaN Laser Lift-off Light-Emitting Diodes Formed by ICP Dry Etching", IEEE Photon. Tech. Lett., V19, N11, p849, (Jun. 1, 2007)

[16] Y. J. Lee, T.C. Lu, H.C. Kuo, and S.C. Wang, "High Brightness GaN-based Light Emitting Diodes", IEEE J. Display Technol. V3, No2, pp118-125, in conjunction with IEEE J. Select. Topics Quantum. Electron., (June, 2007)

[17] T. S. Ko, T. C. Wang, R. C. Gao, H. G. Chen, G. S. Huang, T. C. Lu, H. C. Kuo, and S. C. Wang "Observations on surface morphologies and dislocations of a-plane GaN grown by metal organic chemical vapor deposition", Phys. Stat. Sol. (c), V4, No. 7, pp2510-2514, (May 31, 2007)

[18] T. Wang, T. Ko, H. Kuo, T. Lu, Min Yu, C. Chuo, and Z. Lee, "Optical and structural properties of a-plane GaN with epitaxial lateral overgrowth", Phys. Stat. Sol. (c), V4, No. 7, pp2519-2513, (May 31, 2007)

[19] G. S. Huang, Hou-Guang Chen, J. J. Chen, T. C. Lu, H. C. Kuo, and S. C. Wang, "Hybrid nitride microcavity using crack-free highly reflective AlN/GaN and Ta$_2$O$_5$/SiO$_2$ distributed Bragg mirror", Phys. Stat. Sol. (a), V204, No. 6, pp1977-1981, (May 15, 2007)

[20] T. S. Ko, T. C. Lu, T. C. Wang, M. H. Lo, J. R. Chen, R. C. Gao, H. C. Kuo, S. C. Wang "Optical characteristics of a-plane InGaN multiple quantum wells with different well width", Appl. Phys. Lett., V90, 181122, (Apr. 30, 2007), also selected for the June 2007 issue of Virtual Journal of Ultrafast Science

[21] Hou-Guang Chen, Nai-Fang Hsu, Hsin-Hung Yao, Jung-Tang Chu, Tien-Chang Lu, Hao-Chung Kuo and Shing-Chung Wang, "Strong Ultraviolet Emission from InGaN/AlGaN Multi Quantum Well Grown by Multi-step Process", Jpn. J. Appl. Phys., Vol. 46, No. 4B, pp. 2574-2577 (Apr. 24, 2007)

[22] Yea-Chen Lee, Chia-En Lee, Bo-Siao Cheng, Tien-Chang Lu, Hao-Chung Kuo, Shing-Chung Wang, and Shu-Woei Chiou, "High Performances of 650 nm Resonant Cavity Light Emitting Diodes for Plastic Optical Fiber Application", Jpn. J. Appl. Phys., Vol. 46, No. 4B, pp. 2450-2453 (Apr. 24, 2007)

[23] Y. J. Lee, P.C. Lin, T.C. Lu, H.C. Kuo, and S.C. Wang, "Dichromatic InGaN-based white light-emitting-diodes by using laser lift-off and wafer-bonding scheme", Appl. Phys. Lett., V90, 161115, (Apr. 18, 2007)

[24] H. W. Huang, H. C. Kuo, C. F. Lai, C. E. Lee, C. W. Chiu, T. C. Lu, S. C. Wang, C. H. Lin, and K. M. Leung "High performance GaN-based vertical-injection light-emitting diodes with TiO_2/SiO_2 omni-directional reflector and n-GaN roughness", V19, Issue 18, pp565-567, IEEE Photon. Tech. Lett, (Apr. 15, 2007)

[25] Y. J. Lee, T. C. Lu, H.C. Kuo, S.C. Wang, T. C. Hsu, M. H. Hsieh, M. J. Jou, and B. J. Lee, "Nano-roughening n-side surface of AlGaInP-based LEDs for increasing extraction efficiency", Materials Science and Engineering: B, V138, No2, pp157-160, (March 25, 2007)

[26] P. T. Lee, T. W. Lu, F. M. Tsai, and T. C. Lu, "Lasing Action of Octagonal Quasi-Periodic Photonic Crystal Microcavity," Jpn. J. Appl. Phys., V46, No. 3A, pp971 -973, (Mar. 8, 2007)

[27] G.S. Huang, T. C. Lu, H. H. Yao, H.C. Kuo, S. C. Wang, Greg Sun, Chih-wei Lin, and Li Chang, "Fabrication and characterization of active region of a terahertz GaN/AlGaN quantum cascade laser", J. Crystal Growth, V298, pp687-690,   (Feb. 2007)

[28] Hung-Wen Huang, Chih-Chiang Kao, Jung-Tang Chu, Wei-Chih Wang, Tien-Chang Lu, Hao-Chung Kuo, Shing-Chung Wang, and Chang-Chin Yu, "Investigation of InGaN/GaN Light Emitting Diodes with Nano-roughened surface by Excimer Laser Etching Method", Materials Science and Engineering: B, V136, pp182-186, (Jan, 25, 2007)

[29] T. S. Ko, T. C. Wang, R. C. Gao, H. G. Chen, G. S. Huang, T. C. Lu, H. C. Kuo, and S. C. Wang "Study on optimal growth condition of a-plane GaN grown on r-plane sapphire by MOCVD", J. Crystal Growth, V300, p303-313, (Jan. 20, 2007)

[30] T. S. Ko, T. C. Wang, H. G. Chen, R. C. Gao, Y. J. Lee, T. C. Lu, H. C. Kuo, and S. C. Wan, "InGaN/GaN Nano-stripe Grown on Pattern Sapphire by Metal Organic Chemical Vapor Deposition", Appl. Phys. Lett., V90, 013110, (Jan, 1, 2007)

2008

[1] Chia En Lee, B.S. Cheng, Yea-Chen LeeCE, Hao-Chung Kuo, Tien-chang Lu, and Shing-Chung Wang, "Output Power Enhancement of Vertical-Injection Ultraviolet Light-Emitting Diodes by GaN-Free and Surface Roughness Structures," Electrochem. Solid-State Lett., V12, N12, H44-H46, (Dec. 10, 2008)

[2] Zhen-Yu Li, Wu-Yih Uen, Ming-Hua Lo, Ching-Hua Chiu, Po-Chun Lin, Chih-Tsang Hung, Tien-Chang Lu, Hao-Chung Kuo, Shing-Chung Wang, Yen-Chin Huang, "Enhancing the emission efficiency of $In_{0.2}Ga_{0.8}N/GaN$ MQW blue LED by using appropriately misoriented sapphire substrates," J. Electrochem. Soc., 156, (2), H129-H133, (Dec. 9, 2008)

[3] Yea-Chen Lee, Hao-Chung Kuo, Chia-En Lee, Tien-Chang Lu, and Shing-Chung Wang "High Performances $(Al_xGa_{1-x})_{0.5}In_{0.5}P$-Based Flip-Chip Light-Emitting Diode with a Geometric Sapphire Shaping Structure," IEEE Photon. Tech. Lett., V20 N.23, pp1950-1952, (Dec. 1, 2008)

[4] C. H. Chiu, Zhen-yu Li, C. L. Chao, M. H. Lo, H. C. Kuo, P. C. Yu, T. C. Lu, and S. C. Wang, K. M. Lau, S. J. Cheng, "Efficiency Enhancement of UV/Blue Light Emitting Diodes via Nanoscaled Epitaxial Lateral Overgrowth of GaN on a SiO_2 Nanorod-Array Patterned Sapphire Substrate," J. Crystal Growth, 310 pp5150-5174, (Nov 15, 2008)

[5] Jun-Rong Chen, Shih-Chun Ling, Tsung-Shine Ko, Tien-Chang Lu, Hao-Chung Kuo, and Shing-Chung Wang, "High-reflectivity ultraviolet AlN/AlGaN distributed Bragg reflectors grown by metalorganic chemical vapor deposition," J. Crystal Growth, 310 pp4871-4875 (Nov. 15, 2008)

[6] T. S. Ko, Y. T. Lee, J. R. Chen, S. C. Ling, T. C. Lu, H. C. Kuo, and S. C. Wang "Characteristics of a-plane GaN with SiN_x insertion layer grown by metal-organic chemical vapor deposition," J. Crystal Growth, 310, pp4972-4975, (Nov. 15, 2008)

[7] T. S. Ko, T. C. Lu, T. C. Wang, J. R. Chen, M. H. Lo, R. C. Gao, H. C. Kuo, and S. C. Wang, J. L. Shen "Optical characteristics of *a*-plane InGaN/GaN multiple quantum wells with different well width grown by metal-organic chemical vapor deposition", J. Appl. Phys., 104, 093106, (Nov. 7, 2008) and was selected in Virtual Journal of Ultrafast Science –Volume 7, issue 12 ,Dec, 2008

[8] Z.Y. Li, M. H. Lo, C.T. Hung, S.W. Chen, T. C. Lu, H. C. Kuo and S. C. Wang "High quality ultraviolet AlGaN/GaN multiple quantum wells grown by using atomic layer deposition technique", Appl. Phys. Lett., 93, 131116, (Oct. 3, 2008)

[9] Tien-Chang Lu, Shih-Wei Chen, Tsung-Ting Kao, and Tzu-Wei Liu, "Characteristics of GaN-based photonic crystal surface-emitting lasers", Appl. Phys. Lett., 93, 111111, (Sept. 18, 2008)

[10] Tsung-Shine Ko, Chia-Pu Chu, Jun-Rong Chen, Yu-Cheng Chang, Tien-Chang Lu, Hao-Chung Kuo, and Shing-Chung Wang, "Thermally evaporated In_2O_3 nanoloquats with tunable broad-band emissions", J. NanoSci. and NanoTech., V8, N9, pp4395-4398 (Sept., 2008)

[11] J. R. Chen, T. S. Ko, P. Y. Su, Tien-Chang Lu, Y. K. Kuo, H. C. Kuo, S. C. Wang, "Numerical Study on Optimization of Active Layer Structures for GaN/AlGaN

Multiple-Quantum-Well Laser Diodes," IEEE, J. Lightwave Tech., V26, N.17, pp3155-3165, (Sept. 1, 2009)

[12] Peichen Yu, C. H. Chiu, J. R. Chen, C. C. Kao, H. C. Kuo, T. C. Lu, S. C. Wang, Yuh-Renn Wu, Han-Wei Yang, and W. Y. Yeh "Strain Relaxation Induced Micro-Photoluminescence Characteristics of a Single InGaN-based Nanopillar Fabricated by Focused Ion Beam Milling," Appl. Phys. Lett., 93, 081110, (Aug. 26, 2008) and was selected in Virtual Journal of Nanoscale Science & Technology –Volume 18, issue 10 ,Sept. 8, 2008

[13] Peichen Yu, C. H. Chiu, C. L. Chao, Z. Y. Li, H. C. Kuo, T. C. Lu, S. C. Wang, K. M. Lau, and S. J. Cheng, "Nanoscale Epitaxial Lateral Overgrowth of GaN-based Light Emitting Diodes on a SiO$_2$ Nanorod-Array Patterned Sapphire Template," Appl. Phys. Lett., 93, 081108, (Aug. 26, 2008)

[14] T.C. Lu, J. T. Chu, Bo-Siao Cheng, H.C. Kuo and S.C. Wang, "Lasing behavior, Gain Property and Strong Coupling Effect in GaN-based Vertical-cavity Surface-emitting Lasers," Jpn. J. Appl. Phys., V47, N8, pp6655-6659, (Aug. 22, 2008)

[15] Jun-Rong Chen, Tsung-Shine Ko, Tien-Chang Lu, Yi-An Chang, Hao-Chung Kuo, Yen-Kuang Kuo, Jui-Yen Tsai, Li-Wen Laih and Shing-Chung Wang, "Fabrication and Characterization of Temperature Insensitive 660-nm Resonant-Cavity LEDs", IEEE J. Lightwave Tech., V26, N13, pp1891-1900, (Jul. 1, 2008)

[16] C. H. Chiu, Peichen Yu, H. C. Kuo, C. C. Chen,   T.C. Lu, and S. C. Wang, S. H. Hsu, Y. J. Cheng, and Y. C. Chang "Broad Angular and Spectral Anti-Reflection from GaN Nano-Pillar Surfaces" Opt. Express, V16, N12, p8748-8754 (Jun. 9, 2008)

[17] Ya-Ju Lee, H.C. Kuo, T.C. Lu, and S.C. Wang, Kar Wai Ng, Kei May Lau, Zu-Po Yang, Allan S.P. Chang, and Shawn-Yu Lin, "Study of GaN-based light emitting diodes grown on chemical wet etching patterned sapphire substrate with V-shaped pits roughening surfaces", IEEE J. Lightwave Tech., V21, N11, p1455-1463, (Jun. 1, 2008)

[18] C.H. Chiu, M. H. Lo, T. C. Lu, P. Yu, H.C. Kuo, H. W. Huang, and S.C. Wang, "Nano-processing Techniques Applied in GaN-based Light Emitting Devices with Self-assembly Ni Nano-masks", IEEE J. Lightwave Tech., V26, N11 p1445-1454, (Jun. 1,2008)

[19] B. S. Cheng, C. H. Chiu, K. J. Huang, C. F. Lai, H. C. Kuo, C. H. Lin, T. C. Lu, S. C. Wang, and C. C. Yu, "Enhanced light extraction of InGaN-based green LEDs by nano-imprinted 2D photonic crystal pattern," Semicon. Sci. Tech.,   V23, N5, 055002, (May, 2008)

[20] Chia-En Lee, Yea-Chen Lee, Hao-Chung Kuo, Tien-Chang Lu, and Shing-Chung Wang, "Further Enhancement of Nitride-Based Near-Ultraviolet Vertical-Injection Light-Emitting Diodes by Adopting a Roughened Mesh-Surface," IEEE Photon. Tech. Lett. V20, N10, p803-805 (May15, 2008)

[21] C.H. Lin, H.H. Yen, C.F. Lai, H.W. Huang, C.H. Chao, H.C. Kao, T.C. Lu, S.C. Wang, and K.M. Leung, "Enhanced Vertical Extraction Efficiency From a Thin-Film InGaN–GaN Light-Emitting Diode Using a 2-D Photonic Crystal and an Omnidirectional Reflector," IEEE Photon. Tech. Lett. V20, N10, p836-838 (May 15, 2008)

[22] H. W. Huang, C. H. Lin, C. C. Yu, B. D. Lee, C. H. Chiu, C. F. Lai, H. C. Kuo, K. M. Leung, T. C. Lu, and S. C. Wang, "Enhanced light output from a nitride-based power chip of green light-emitting diodes with nano-rough surface using nanoimprint lithography," Nanotechnology, V19, 185301 (May 7, 2008)

[23] H W Huang, C H Lin, C C Yu, B D Lee, C H Chiu, C F Lai, H C Kuo, K M Leung, T C Lu and S C Wang, "Improvement of light output in GaN-based power chip light-emitting diodes with a nano-rough surface by nanoimprint lithography,", Semicon. Sci. Tech., V23, N5, 055002, V23, N10, 045022, (Apr., 2008)

[24] Y C Lee, C E Lee, T C Lu, H C Kuo and S C Wang, " Small GaN-based light-emitting diodes with a single electrode pad fabricated on a sapphire substrate," Semicon. Sci. Tech., V23, N5, 055002, V23, N4, 045013, (Apr., 2008)

[25] S.-L. Wang, B.-C. Yeh, H.-M. Wu, L.-H. Peng, C.-M Lai, T.-S Ko, T.-C Lu, S.-C Wang, and A.-H Kung, "Optical properties of *a*-plane GaN strained by photo- chemically grown gallium hydroxide", Phys. Stat. Sol. (c) 5 No.6, 1780 (Apr. 21, 2008)

[26] Te-Chung Wang, Tsung-Shine Ko, Tien-Chang Lu, Hao-Chung Kuo, Run-Ci Gao, Jenq-Dar Tsay, and Sing-Chung Wang, "Internal quantum efficiency behavior of a-plane and c-plane InGaN / GaN multiple quantum well with different indium compositions", Phys. Stat. Sol. (c) 5 No. 6, 2161 (Apr. 17, 2008)

[27] Chia-En Lee, Yea-Chen Lee, Hao-Chung Kuo, Tien-Chang Lu, and Shing-Chung Wang, "High-brightness InGaN-GaN flip-chip light-emitting diodes with triple-light scattering layers," IEEE Photon. Tech. Lett., V20, N8, p659-661 (Apr. 15, 2008)

[28] S. C. Lin, T. C. Wang, T. S. Ko, T. C. Lu, H. C. Kuo and S. C. Wang, "Characteristics of ultraviolet nonpolar InGaN/GaN light-emitting diodes using trench epitaxial lateral overgrowth technology", J. Crystal Growth 310, 2330, (Apr. 2008)

[29] Ching-Hua Chiu, Chia-En Lee, Ming-Hua Lo, Hung-Wen Huang, Tien-Chang Lu, Hao-Chung Kuo and Shing Chung Wang "Metal organic chemical vapor deposition growth of GaN-based light emitting diodes with naturally formed nano pyramids", Jpn. J. Appl. Phys., V47, N4, p2954-2956 (Apr. 2008)

[30] Tien-Chang Lu, Chih-Chiang Kao, Hao-Chung Kuo, Gen-Sheng Huang, and Shing-Chung Wang "CW Lasing of Current Injection Blue GaN-Based Vertical Cavity Surface Emitting Laser", Appl. Phys. Lett., 92 141102 (Apr. 7, 2008)

[31] Tsung-Shine Ko, Chia-Pu Chu, Jun-Rong Chen, Yu-Cheng Chang, Tien-Chang Lu, Hao-Chung Kuo, and Shing-Chung Wang, "Tunable light emissions from thermally evaporated In_2O_3 nanostructures grown at different growth temperatures", J. Crystal Growth 310, 2264, (Apr. 2008)

[32] Hou-guan Chen, Tsung-shine Ko, Li Chang, Yue-han Wu, Tien-Chang Lu, Hao-chung Kuo, and Shing-chung Wang, "Investigation on microstructure in GaN epitaxial growth on the striped patterned r-plane sapphire substrates", J. Crystal Growth, 310, 1627, (Apr. 2008)

[33] T. S. Ko, J. Shieh, M. C. Yang, T. C. Lu, H. C. Kuo, and S. C. Wang, "Phase transformation and optical characteristics of porous germanium thin film", Thin Solid Film, 516, 2934 (March, 2008)

[34] Y.C. Lee, C.E. Lee, H.C. Kuo, T. C. Lu, and S.C. Wang, "Enhancing the Light Extraction of $(Al_xGa_{1-x})_{0.5}In_{0.5}P$ Based Light-Emitting Diode Fabricated Via Geometric Sapphire Shaping", IEEE Photon. Tech. Lett., V20, N5, p369-371, (Mar. 1, 2008)

[35] Y.C. Lee, C.E. Lee, H.C. Kuo, T. C. Lu, and S.C. Wang, "High brightness GaN-based flip-chip light-emitting diodes by adopting geometric sapphire shaping structure," Semicon. Sci. Tech., V23 N2 025015 (Feb, 2008)

[36] Chia-Pu Chu, Tsung-Shine Ko, Tien-Chang Lu, Hao-Chung Kuo, and Shing-Chung Wang, "Thermally evaporated In_2O_3 nanoloquats with tunable broad-band emissions", Materials Science and Engineering: B, V147, N. 2-3, p276, (Feb. 15, 2008)

[37] Jun-Rong Chen, Chung-Hsien Lee, Tsung-Shine Ko, Yi-An Chang, Tien-Chang Lu, Hao-Chung Kuo, Yen-Kuang Kuo, and Shing-Chung Wang, "Effects of Built-In Polarization and Carrier Overflow on InGaN Quantum-Well Lasers with Electronic Blocking Layer", IEEE J. Lightwave Tech., 26 No.3, 329 (Feb. 1, 2008)

[38] C. E. Lee, H. C. Kuo, Y. C. Lee, M. R. Tsai, T. C. Lu, S. C. Wang, and C. T. Kuo, "Luminance Enhancement of Flip-Chip Light-Emitting Diodes by Geometric Sapphire Shaping Structure", IEEE Photon. Tech. Lett., V20, N3, p184-186, (Feb. 1, 2008)

[39] C. H. Chiu, C. E. Lee, C.L. Chao, B. S. Cheng, H.W. Huang, H. C. Kuo, T. C. Lu, S. C. Wang, W. L. Kuo, C. S. Hsiao and S. Y. Chen "Enhancement of light output intensity by integrating ZnO nanorod arrays on GaN-based laser lift-off vertical light emitting diodes", Electrochem. Solid-State Lett., 11, Issue 4, H84-H87 (Jan. 30, 2008)

[40] T. C. Lu, S. W. Chen, L. F. Lin, T. T. Kao, C. C. Kao, P. C. Yu, H. C. Kuo, S. C. Wang and S. H. Fan, "GaN-based two-dimensional surface-emitting photonic crystal lasers with AlN/GaN distributed Bragg reflectors", Appl. Phys. Lett., 92, 011129 (Jan. 2008) and was selected in Virtual Journal of Nanoscale Science & Technology – Jan. 21, 2008 issue

2009

[1] Shih-Chun Ling, C. L. Chao, Jun-Rong Chen, Tsung-Shine Ko, Tien-Chang Lu, Hao-Chung Kuo, Shing-Chung Wang, Po-Chun Liu and Jenq-Dar Tsay, "Nano-rod epitaxial lateral overgrowth of a-plane GaN with low dislocation density," Applied Physics Letter, Vol. 94, pp. 251912 (2009)

[2] Shih-Chun Ling, Te-Chung Wang, Jun-Rong Chen, Tsung-Shine Ko, Bao-Yao Chang, Tien-Chang Lu, Hao-Chung Kuo, Shing-Chung Wang, Po-Chun Liu and Jenq-Dar Tsay, "Characteristics of a-plane green light emitting diode grown on r-plane sapphire," IEEE Photonics Technology Letters, Vol. 21, pp. 1130-1132 (2009)

[3] F. I. Lai, S. C. Ling, C. E. Hsieh, T. H. Hsueh, H. C. Kuo, and T. C. Lu, "Extraction Efficiency Enhancement of GaN-Based Light Emitting Diodes by Micro-hole Array and Roughened Surface Oxide," accepted and to be published in IEEE Electron. Device Lett., (2009)

[4] Chun-Feng Lai, Jim-Yong Chi, Hsi-Hsuan Yen, Chia-En Lee, Chia-Hsin Chao, Hao-Chung Kuo, Wen-Yung Yeh, and Tien-Chang Lu, "Far field and near field distribution of GaN-based photonic crystal light-emitting diodes with guided mode extraction," IEEE Journal of Selected Topics in Quantum Electronics, Vol. 15, pp. 1234 (2009)

[5] Min-An Tsai, Peichen Yu, J. R. Chen, J. K. Huang, C. H. Chiu, H. C. Kuo, T. C. Lu, S. H. Lin, and S. C. Wang, "Improving Light Output Power of the GaN-Based Vertical-Injection Light Emitting Diodes by Mg$^+$ Implanted Current Blocking Layer," IEEE Photonics Technology Letters, Vol. 21, pp. 688-690 (2009)

[6] Jun-Rong Chen, Yung-Chi Wu, Tien-Chang Lu, Hao-Chung Kuo, Yen-Kuang Kuo, and Shing-Chung Wang, "Numerical Study on Lateral Mode Behavior of 660-nm InGaP/AlGaInP Multiple-Quantum-Well Laser Diodes", Optical Review, Vol. 16, pp. 375-382 (2009)

[7] Ya-Ju Lee, C. H. Chiu, P. C. Lin, T. C. Lu, H. C. Kuo and S. C. Wang, "Study of the Excitation Power Dependent Internal Quantum Efficiency in InGaN/GaN LEDs Grown on Patterned Sapphire Substrate," IEEE Journal of Selected Topics in Quantum Electronics, Vol. 15, pp. 1137 (2009)

[8] Tien-Chang Lu, Jun-Rong Chen, Shih-Wei Chen, Hao-Chung Kao, Chien-Cheng Kuo, Cheng-Chung Lee, and Shing-Chung Wang, "Development of GaN-Based Vertical-Cavity Surface-Emitting Lasers," IEEE Journal of Selected Topics in Quantum Electronics, Vol. 15, pp. 850 (2009)

[9] S. W. Chen, T. C. Lu, and T. T. Kao, "Study of GaN-based Photonic Crystal Surface Emitting Lasers with AlN/GaN Distributed Bragg Reflectors," IEEE Journal of Selected Topics in Quantum Electronics, Vol. 15, pp. 885 (2009)

[10] Y. C. Lee, C. E. Lee, H.C. Kuo, T. C. Lu, S. C. Wang, "High Performance 650 nm Resonant-Cavity Light-Emitting Diodes Fabricated on Si Substrate by Twice Wafer Bonding Techniques", accepted and to be published in Semicon. Sci. Tech., (2009)

[11] Shih-Chun Ling, Te-Chung Wang, Tsung-Shine Ko, Jun-Rong Chen, Tien-Chang Lu, Hao-Chung Kuo, Shing-Chung Wang and Jenq-Dar Tsay "Performance enhancement of a-plane light-emitting diodes using InGaN/GaN superlattices" Jpn. J. Appl. Phys., V48, 04C136, (Apr. 20, 2009)

[12] S. W. Chen, M. H. Lo, T. T. Kao, C. C. Kao, J. T. Chu, L. F. Lin, H. W. Huang, T. C. Lu, H. C. Kuo, S. C. Wang, C. C. Kuo, and C. C. Lee, "Effects of Inhomogeneous Gain and Loss on Nitride-based Vertical-Cavity Surface Emitting Lasers" Jpn. J. Appl. Phys., V48, 04C127, (Apr. 20, 2009)

[13] Bo-Siao Cheng, Chia-En Lee, Hao-Chung Kuo, Tien-Chang Lu, and Shing-Chung Wang, "Power Enhancement of GaN-Based Flip-Chip Light-Emitting Diodes with Triple Roughened Surfaces," Jpn. J. Appl. Phys., V48, 04C115, (Apr. 20, 2009)

[14] Ya-Ju Lee, S. Y. Lin, C. H. Chiu, T. C. Lu, H. C. Kuo, S. C. Wang, and E. F. Schubert "High Output Power Density from GaN-based Two-dimensional Nanorod Light-Emitting Diode Arrays," Appl. Phys. Lett., V94, 141111, (Apr. 10, 2009)

[15] J.R. Chen, S.C. Ling, H.M. Huang, P.Y. Su, T.S. Ko, T.C. Lu, H.C. Kuo, Y.K. Kuo, and S.C. Wang, "Numerical study on optical properties of InGaN multi-quantum-well laser diodes with polarization-matched AlInGaN barrier layers," Appl. Phys. B, V95, N1, p145~153, (Apr. 2009)

[16] C.H. Chiu, S. Y. Kuo, M. H. Lo, T.C. Wang, Y. T. Lee, H. C. Kuo, T. C. Lu, and S. C. Wang, "Optical Properties of a-plane InGaN/GaN Multiple Quantum Wells on r-plane Sapphire Substrates with Different Indium Compositions," J. Appl. Phys., V105, N6, 063105 (Mar. 15, 2009)

[17] C. E. Lee, C. F. Lai, Y. C. Lee, H. C. Kuo, T. C. Lu, and S. C. Wang, "Nitride-Based Thin-Film Light-Emitting Diodes with Photonic QuasiCrystal Surface," IEEE Photon. Tech. Lett., V21, N5, p331~333 (Mar. 1, 2009)

[18] Jun-Rong Chen, Tien-Chang Lu, Yung-Chi Wu, Shiang-Chi Lin, Wei-Rein Liu, and Wen-Feng Hsieh, Chien-Cheng Kuo, and Cheng-Chung Lee, "Large vacuum Rabi splitting in ZnO-based hybrid microcavities observed at room temperature," V94, 061103, Appl. Phys. Lett., (Feb. 9, 2009)

[19] Min-An Tsai, Peichen Yu, C. L.Chao, C. H. Chiu, H. C. Kuo, S. H. Lin, J. J. Huang, T. C. Lu, and S. C. Wang, "Efficiency Enhancement and Beam Shaping of GaN-InGaN Vertical-Injection Light-Emitting Diodes via High-Aspect-Ratio Nanorod Arrays," IEEE Photon. Tech. Lett., V21, N1~5, p257~259 (Jan-Fab, 2009)

[20] Z. Y. Li, T. C. Lu, H. C. Kuo, S. C. Wang M. H. Lo, and K. M. Lau "HRTEM investigation of high reflectance AlN/GaN Distributed Bragg Reflectors by inserting AlN/GaN supperlattice," J. Crystal Growth, V311 p3089-3092, (Jan. 21, 2009)

[21] M. D. Yang, Y. W. Liu, J. L. Shen, C. W. Chen, G. C. Chi, T. Y. Lin, W. C. Chou, M. H. Lo, H. C. Kuo, and T. C. Lu, "Density-dependent energy relaxation of hot electrons in InN epilayers," J. Appl. Phys., V105, 013526, (Jan. 9, 2009)

[22] Z. Y. Li, M. H. Lo, C. H. Chiu, P. C. Lin, T. C. Lu, H. C. Kuo, S. C. Wang, "Carrier localization degree of InGaN/GaN multiple quantum wells grown on vicinal sapphire substrates," J. Appl. Phys., V105, 013103, (Jan. 6, 2009)

參加日本國際奈米展心得報告

報告人：陳士偉，Chen Shih Wei

交通大學光電工程研究所博士班四年級

參加會議過程：

日本國際奈米展為全世界最著名的展覽會之一，每年都在日本台場的國際會議舉行。此會議是因應全世界對於光電元件的發展甚至越來越普以及重要性的奈米結構或材料之應用商品，今年展覽的日期為 2 月 18 日至 2 月 20 日。本次展覽由日本國際貿易協會主辦，為國際知名且最重要的展覽會之一。本次展覽邀請全世界著名的廠商與學校共同參加本次展覽，同時分為許多館區，如加拿大、美國、英國、台灣或韓國等等...。參觀人數多達數萬名來自世界各地包跨美國、日本、加拿大及歐洲的知名廠商與日本各級學校，裡面更有許多種類的商品利用不同的奈米結構製作並且首次在本展覽會中發表，如碳 60 奈米結構或利用奈米碳管製作場發射顯示器等等...；此外，在本次的展覽會中亦介紹一些有機發光二極體的應用等等，代表未來的有機發光二極體具有極高發展潛力，相關的廠商應注意相關的研究與發展。

本次的展覽會中，有許多公司展覽並報告各公司的研究成果，其中以參展廠商 Toshiba 所報告的紫外光發光二極體的研究對於我們交通大學半導體雷射實驗室中，發光二極體研究的領域具有非常重要的關係。本實驗室的發光二極體研究已經耕耘了近十餘年，具有相當不錯的結果並且發表許許多多文章在各級高影響力的期刊。在本次研討會中 Toshiba 公司演講的題目為紫外光發光二極體的發展潛力與應用。內容包含如何製作紫外光發光二極體，接著介紹目前的最新進展，並且顯示在不同的電流密度注入下的發光強度，最後介紹紫外光的發光二極體在未來生醫以及照明的應用。其中以如何製作高功率的紫外光發光二極體，以及高溫度的氮化鋁材料的成核層的重要性，此一方面與本實驗室所研發的結構與材料息息相關，更揭露未來 Toshiba 對此方面的最新進展以及重視程度。

本次展覽會我們也展示氮化鎵發光二極體以及雷射結構的實驗結果，量測的結果與使用的技術不但是全台灣第一顆元件，更是領先全

球的結果。同時，合作廠商更展示出全世界第一家公司利用奈米壓印技術製作光子晶體發光二極體的結構。因此在本次展覽會中，有許多有興趣的廠商紛紛詢問相關技術內容以及參觀實體元件，對於廠商商品之推廣具有相當大的幫助。

由於本實驗室與日本 Canon 公司有合作計畫，因此利用本次展覽會的展覽期間討論相關的合作事項以及內容，希望藉此增進本實驗室與日本 Canon 公司之間的加強合作，希望能將製作出氮化鎵垂直型共振腔面射型雷射搭配混合型布拉格反射鏡之元件，本人也與日本 Canon 的加藤部長討論相關事項，彼此間的互動性討論相當多，他們也給予我不少的建議與提供我許多在本次元件設計中不足的地方，這些都能給我非常多的思考與想法，近一步增進對於本結構，或是對於國際間未來的發展趨勢更深一層的想法與思考。相信對於未來的研究會有更進一步的進展。
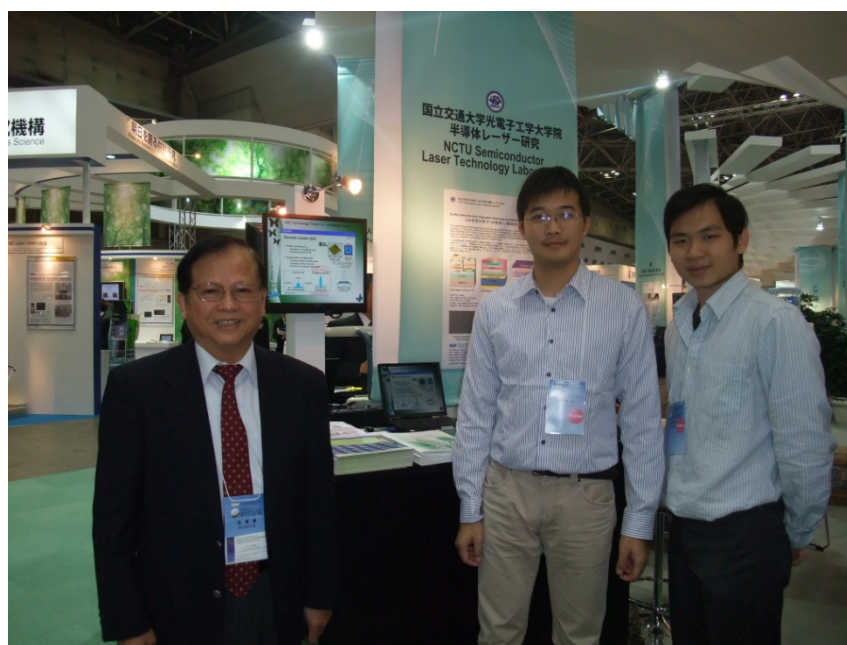
圖一、本次展覽攤位與王興宗教授合照
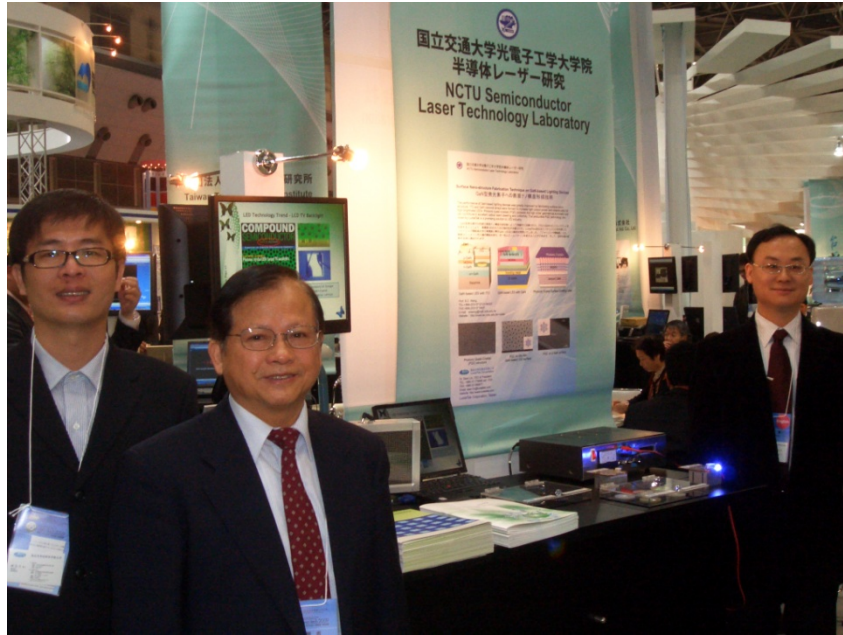
圖二、本次展覽攤位之旭晶光合作廠商與王興宗教授合照

圖三、Toshiba 攤位之展覽與介紹

參加美國國際材料科學研討會心得報告

報告人：陳俊榮，Jun-Rong Chen

交通大學光電工程研究所博士班四年級

參加會議過程：

我們一行人由桃園搭乘國內長榮航空公司班機至舊金山，航程大約 11 小時，至舊金山後搭乘與機場連接之捷運系統 BART 至 Powell 站後，即可至 MRS 的會議地點 Moscone West，會場大廳如圖一所示。第一天到達後已是當地時間的下午 4 點，考量時間問題，我們便先行至預定的旅館 check in 與調整時差。第二天上午，我們先至會場進行會議註冊與確定口頭報告的會議廳位置。

會議的第二天一早，我們便再次前往會場，由於同行的實驗室同學之一在第二天有口頭報告，我們便提早至會場準備上傳報告所需的檔案。此外，在選擇一些與本身研究領域相關的演講之後，我們還特別針對許多研究群最近的研究結果進行整理與資料蒐集。另外有一些著名的國外研究群之研究結果，也被大會選為邀請演講，邀請演講一般為 30 分鐘，一般演講則為 15 分鐘。第二天的會議演講我們主要針對氮化物發光二極體的相關演講內容進行聆聽。

會議的第三天，我們便繼續聆聽相關的論文報告，並在下午參觀會場中所舉辦的材料分析與成長等相關儀器設備商的展覽。其中像是 AIXTRON 與 VEECO 等 MOCVD 的兩大廠商都有參與展覽。此外例如材料分析所需的相關儀器，如 AFM，XRD 與 SEM 等，都有許多相關的展示，亦讓我們得知材料分析儀器的最新發展。再參觀完儀器展示後第四天的會議，便是我要上台口頭報告的時間，我的演講時間是早上 9:30 分，但必須提早在八點左右上傳檔案。報告過程十分順利，報告結束後亦有主持人與另一位外國學者分別針對我的研究內容提問，回答過程也十分順利。下午我們則前往壁報論文的會場，由於此項會議是材料領域的重大會議，而材料所包含的領域更是十分廣泛，所以會議進行過程中將近有二十個會議廳同時進行，不同國家前來的研究人員亦是在會場中到處可見。

會議之後，我們則安排考察參觀加州大學聖塔芭芭拉分校。由於在氮化物和三五族半導體材料中，加州大學聖塔芭芭拉分校占有相當重要的地位，包括 Prof. Nakamura, Prof. Coldren, Prof. Evelyn Hu 與 Prof. DenBaars 都是三五族材料的重要研究群，由於在加州大學聖塔芭芭拉分校有之前交通大學材料所的學生與本實驗室已畢業的學姐，在他們的帶領下，我們參觀了許多研究設備，包括無塵室，分子束磊晶設備等，受益良多。

2009 Materials Research Society (MRS)會議是全球材料領域最重要的會議之一，經由參加這次會議，讓我學習到國外大型國際研討會的進行方式，此外，這次出國的經驗，亦讓我體會到包括語言及社會文化與生活習慣的差異。在到達美國舊金山之後，我發現當地的建築與街道都與台灣有相當大的差異，當地天氣幾乎每天都是晴朗的好天氣，更體會加州陽光的美，在舊金山的交通也十分方便，有地下捷運 BART，還有舊金山最著名的 Cable Car，它是利用地下纜線的方式進行運輸，非常特別。而各項交通資訊的標示也十分清楚。

圖一、MRS 舊金山會議中心

圖二、與王興宗老師在 MRS 會場的合照